

# A morphological study of galaxies in ZwCl0024+1652, a galaxy cluster at redshift $z \sim 0.4$

Zeleke Beyoro Amado,<sup>1,2\*</sup> Mirjana Pović,<sup>1,3</sup> Miguel Sánchez-Portal,<sup>4,5,6</sup>  
S. B. Tessema,<sup>1</sup> Ángel Bongiovanni,<sup>7,8,9</sup> Jordi Cepa,<sup>7,8,9</sup> Miguel Cerviño,<sup>10</sup>  
J. Ignacio González-Serrano,<sup>11</sup> Jakub Nadolny,<sup>7,8</sup> Ana Maria Pérez Garcia,<sup>12</sup>  
Ricardo Pérez-Martínez<sup>13</sup> and Irene Pintos-Castro<sup>14</sup>

<sup>1</sup>Astronomy and Astrophysics Research and Development Division, Ethiopian Space Science and Technology Institute (ESSTI), Entoto Observatory and Research Centre (EORC), PO Box 33679 Addis Ababa, Ethiopia

<sup>2</sup>Department of Physics, College of Natural and Computational Sciences, Kotebe Metropolitan University, PO Box 31248 Addis Ababa, Ethiopia

<sup>3</sup>Instituto de Astrofísica de Andalucía (IAA-CSIC), Glorieta de la Astronomía s/n, E-18008 Granada, Spain

<sup>4</sup>Instituto de Radioastronomía Milimétrica, Av. Divina Pastora 7, Núcleo Central, E-18012 Granada, Spain

<sup>5</sup>European Southern Observatory, Alonso de Córdova 3107, Vitacura, Santiago 763-0355, Chile

<sup>6</sup>Joint ALMA Observatory, Alonso de Córdova, 3107, Vitacura, Santiago 763-0355, Chile

<sup>7</sup>Instituto de Astrofísica de Canarias (IAC), E-38200 La Laguna, Tenerife, Spain

<sup>8</sup>Departamento de Astrofísica, Universidad de La Laguna (ULL), E-38205 La Laguna, Tenerife, Spain

<sup>9</sup>Asociación Astrofísica para la Promoción de la Investigación, Instrumentación y su Desarrollo, ASPID, E-38205 La Laguna, Tenerife, Spain

<sup>10</sup>Centro de Astrobiología (CSIC/INTA), E-28850 Torrejón de Ardoz, Madrid, Spain

<sup>11</sup>Instituto de Física de Cantabria (CSIC – Universidad de Cantabria), Avda. de los Castros s/n, E-390055 Santander, Spain

<sup>12</sup>Centro de Astrobiología (CSIC/INTA), ESAC Campus, Camino Bajo del Castillo s/n, E-28692 Villanueva de la Cañada, Spain

<sup>13</sup>ISDEFE for ESA, Camino Bajo del Castillo s/n, Urb. Villafranca del Castillo, E-28692 Villanueva de la Cañada, Spain

<sup>14</sup>Department of Astronomy & Astrophysics, University of Toronto, 50 St. George Street, Toronto, ON M5S 3H4, Canada

Accepted 2019 February 7. Received 2019 February 7; in original form 2018 November 25

## ABSTRACT

The well-known cluster of galaxies ZwCl0024+1652 at  $z \sim 0.4$  lacks an in-depth morphological classification of its central region. While previous studies provide a visual classification of a patched area, we used the public code called galaxy Support Vector Machine (GALSVM) and *HST*/ACS data as well as the WFP2 master catalogue to automatically classify all cluster members up to 1 Mpc. GALSVM analyses galaxy morphologies through support vector machine (SVM). From the 231 cluster galaxies, we classified 97 as early types (ETs) and 83 as late types (LTs). The remaining 51 stayed unclassified (or undecided). By cross-matching our results with the existing visual classification, we found an agreement of 81 per cent. In addition to previous ZwCl0024 morphological classifications, 121 of our galaxies were classified for the first time in this work. In addition, we tested the location of classified galaxies on the standard morphological diagrams, colour–colour and colour–magnitude diagrams. Out of all cluster members,  $\sim 20$  per cent are emission-line galaxies, taking into account previous GLACE results. We have verified that the ET fraction is slightly higher near the cluster core and decreases with the clustercentric distance, while the opposite trend has been observed for LT galaxies. We found a higher fraction of ETs (54 per cent) than LTs (46 per cent) throughout the analysed central region, as expected. In addition, we analysed the correlation between the five morphological parameters (Abraham concentration, Bershady–Concelice concentration, asymmetry, Gini, and M20 moment of light) and the clustercentric distance, without finding a clear trend. Finally, as a result of our work, the morphological catalogue of 231 galaxies containing all the measured parameters and the final classification is available in the electronic form of this paper.

**Key words:** ZwCl0024+1652 – galaxy cluster – galaxies – Morphology – Early-Type – Late-Type – GALSVM – Morphological fraction.

\* E-mail: [zbamado@gmail.com](mailto:zbamado@gmail.com)

## 1 INTRODUCTION

A consolidated observational fact is the outstanding difference in the properties of galaxies located in the cores (or regions of high local galaxy density) and in the external parts (or low-density ones) of low- and intermediate-redshift clusters: The former regions are dominated by red, massive, and passive early-type galaxies (ET galaxies, comprising ellipticals and S0 galaxies), while a substantial increase of the fraction of late-type galaxies (LTs, comprising spiral and irregular objects) is observed in the latter galaxies. This was early identified by Zwicky (1942), and quantified by Dressler (1980) in the so-called morphology–density relation linking the increasing fraction of ET galaxies with the local galaxy density. Similarly, a decrease of the fraction of star-forming (SF) galaxies is observed with increasing local galaxy density [the star formation–density relation; see for instance Pintos-Castro et al. 2013, and references therein]. Moreover, these relations evolve with cosmic time, as was realized by Butcher & Oemler (1978), who found that cluster galaxy populations evolve as the redshift changes in such a way that rich clusters at higher redshifts ( $z > 0.2$ ) are populated with a higher fraction of blue galaxies than low-redshift clusters. This is the so-called Butcher–Oemler (BO) effect. Likewise, an increase of the cluster SF and active galactic nucleus (AGN) activity is observed (see for instance Haines et al. 2009; Martini et al. 2013).

The morphology–density relation seems to hold from nearby clusters up to redshifts as high as  $z \sim 1.5$  (e.g. Dressler et al. 1997; Postman et al. 2005; Holden et al. 2007; Mei et al. 2012; Nantais et al. 2013). Likewise, star formation takes place in low-density regions where LTs dominate while high-density regions are dominated by quiescent ET galaxies since  $z \sim 1.5$  to the local Universe (e.g. Postman & Geller 1984; Kauffmann et al. 2004; Cooper et al. 2012; Wetzel, Tinker & Conroy 2012; Woo et al. 2013). At higher redshifts, there is some controversial evidence of the existence of a reversal of the SF–density relation: Some authors, for example Tran et al. (2010), found an increase (even more dramatic) of the fraction of SF galaxies from low- to high-density regions in clusters at  $z \sim 1.6$ , while other authors (e.g. Ziparo et al. 2014) did not find clear evidence of such type of reversal when studying clusters at the same redshift. Quadri et al. (2012), using mass-selected samples from the UKIDSS Ultra-Deep Survey, conclude that galaxies with quenched SF tend to reside in dense environments out to at least  $z \sim 1.8$ .

The structural and morphological properties of a galaxy are important tracers of its evolutionary stage. Thus, the correlation of the morphology (and/or SF activity) of the clusters’ galaxies with the local density provides valuable information on the stage of infall at which galaxies experience the bulk of their transformations. To this end, it is important to perform wide-area surveys (to study the density-dependent effects) in clusters that span a range of redshifts (to assess the evolution with cosmic time).

The morphological taxonomy of galaxies can be backdated to Reynolds (1920). Visual inspection is the traditional method, and even now a very common way to perform morphological classification of galaxies (e.g. Lintott et al. 2008; Nair & Abraham 2010; Fasano et al. 2012; Kocevski et al. 2012; Kartaltepe et al. 2012, 2015; Buitrago et al. 2013; Willett et al. 2013, 2017; Kuminski & Shamir 2016; Simmons et al. 2017). One of the drawbacks of the visual classification method is its subjectivity, which can be alleviated by performing multiple instances of the classification of each object carried out by different persons; an outstanding example is the Galaxy Zoo project (Lintott et al. 2008, 2011).

In the framework of this ‘citizen science’ initiative, nearly one million galaxies from the Sloan Digital Sky Survey (SDSS) were classified by  $\sim 10^5$  participants who performed more than  $4 \times 10^7$  classifications. Needless to say, when dealing with a large number of sources, the visual classification method can be really time-consuming. It works well for closer and well-resolved objects for accurate estimation. For such objects it agrees with the results of modern classification methods.

But with the currently overgrowing observational astronomical data, the above method is probably not the most appropriate or is even unfeasible for high-redshift galaxies. Modern classification techniques include galaxy-fitting algorithms, which can give reliable results for a large number of galaxies in a relatively shorter period and with minimal human resources. To deal with fast-growing and big astronomical data, machine learning techniques employing convolutional neural networks (CNNs) have been widely used recently for morphological classification of galaxies (e.g. Banerji et al. 2010; Kuminski et al. 2014; Dieleman, Willett & Dambre 2015; Huertas-Company et al. 2015; Aniyani & Thorat 2017; Domínguez et al. 2018; Lukic et al. 2018). Modern galaxy classification methods can be either *parametric* or *non-parametric*.

*Parametric methods* use some parameters of galaxies to classify them by fitting (one- or two-dimensional) mathematical models to their images assuming some pre-defined parametric model. In this approach the Sérsic profile (Sérsic 1963) and a two-component profile (bulge + disk decomposition) are the commonly used models. The classification is obtained by fitting a two-component profile as described in detail by Simard et al. (2002) and Peng et al. (2002). More recently, Simard et al. (2011) have performed a classification of 1.12 million galaxies using a bulge + disc decomposition approach with SDSS data release 7 (Abazajian et al. 2009). In addition to this, a structural and morphological catalogue of 45 million sources has been presented by Tarsitano et al. (2018) with the Dark Energy Survey (The DES Collaboration 2016) data of the first-year observation employing both a single Sérsic parametric fit and non-parametric methods. A parametric method in general is useful in that it gives a complete set of parameters describing the quantitative morphology. Since a large number of parameters need to be fitted, the results may be degenerated, as shown in Huertas-Company et al. (2007). Degeneracy occurs as a result of correlation between parameters, the results of the local minima in the parameter space of the chi-square minimization, or numerical divergence in the process of fitting (Peng et al. 2002, 2010). The peculiar characteristic of the parametric method in general is the assumption that a galaxy is described well by a simple analytic model whereas this does not always work for well-resolved as well as irregular and merging/interacting galaxies.

On the other hand, the *non-parametric* approach does not assume any specific analytic model and is performed on the basis of measuring a set of well-chosen observables. The effects of seeing, being one of the major challenges in galaxy fitting, are not included in non-parametric measurements unlike the parametric ones where the assumed mathematical model is convolved with the point spread function. The non-parametric method was introduced for the first time by Abraham et al. (1994, 1996) with the definition of two observables: the Abraham concentration index and asymmetry. A third quantity, namely smoothness, was introduced by Conselice et al. (2000, 2003). The classification has been further enhanced with additional observables: the GINI coefficient (Abraham, van den Bergh & Nair 2003); the M20 moment of light (Lotz, Primack & Madau 2004), and the Conselice–Bershady concentration (Bershady, Jangren & Conselice 2000; Conselice et al. 2000). These six

parameters, together with ellipticity, are described in more detail in Section 3.3. *Non-parametric* methods are in advantage when classifying a large sample of galaxies at higher redshifts, when lower resolution data are available (e.g. Scarlata et al. 2007; Tasca et al. 2009; Pović et al. 2009, 2013, 2015; Pintos-Castro et al. 2016). Furthermore, no analytic pre-defined profile is required in this approach.

In this paper, we apply a *non-parametric* classification method to a well-known intermediate redshift cluster, namely ZwCl0024+1652, at  $z = 0.395$ . This cluster has been extensively studied by several groups (e.g. Morrison et al. 1997; Broadhurst et al. 2000; Kneib et al. 2003; Treu et al. 2003; Moran et al. 2007; Geach et al. 2009; Natarajan et al. 2009; Sánchez-Portal et al. 2015). In particular, it has been observed by our team in the framework of the GaLaxy Cluster Evolution Survey (GLACE; Sánchez-Portal et al. 2015) in the  $H\alpha$  and  $[NII]$  emission lines to trace the SF and AGN activity in a wide range of environments (see Section 5 below). Although this cluster has been deeply studied in some aspects, a visual morphological classification has been performed for a limited number (214) of member galaxies within a clustercentric distance extending to 5 Mpc (Moran et al. 2007). The purpose of this work is to improve the knowledge about the morphological properties of the member galaxies by providing a reliable classification of the sources up to 1 Mpc of clustercentric radius. We use publicly available *Hubble Space Telescope* (*HST*) Advance Camera for Survey (ACS) data in the F775W filter.

Only 66 galaxies have been classified by Moran et al. (2007) within this radius ( $\approx 31$  per cent of the total sample). The second important objective of this work is to compare the visual classification of Moran et al. (2007) with our *non-parametric* method – this may provide us with a handy tool for future works at higher redshifts.

In this work, we use a *non-parametric* method called GALSVM introduced by Huertas-Company et al. (2008). GALSVM fits a number of parameters simultaneously and assigns probabilities for each galaxy to be classified. Then, based on the probabilities, the galaxies are classified into two broad morphological classes, namely early type and late type. For more details about this classification, we refer the reader to Section 3.5.

The paper is organized as follows: Section 2 describes the data, along with providing a brief description of the generated source catalogue. In Section 3 the GALSVM code and its application to our sample are described. The analyses on the results from our classification are further developed in Section 4. A detailed discussion is presented in Section 5. Finally Section 6 presents brief conclusions of this work.

The following cosmological parameters are assumed throughout this paper:  $\Omega_M = 0.3$ ,  $\Omega_\Lambda = 0.7$ ,  $\Omega_k = 0$ , and  $H_0 = 70 \text{ km s}^{-1} \text{ Mpc}^{-1}$ . All magnitudes are given in the AB system as described by Oke & Gunn (1983), unless otherwise stated.

## 2 DATA

### 2.1 *HST*/ACS data

We used the public *HST* reduced scientific image of ZwCl0024+1652<sup>1</sup> from the observation made on 2004 November

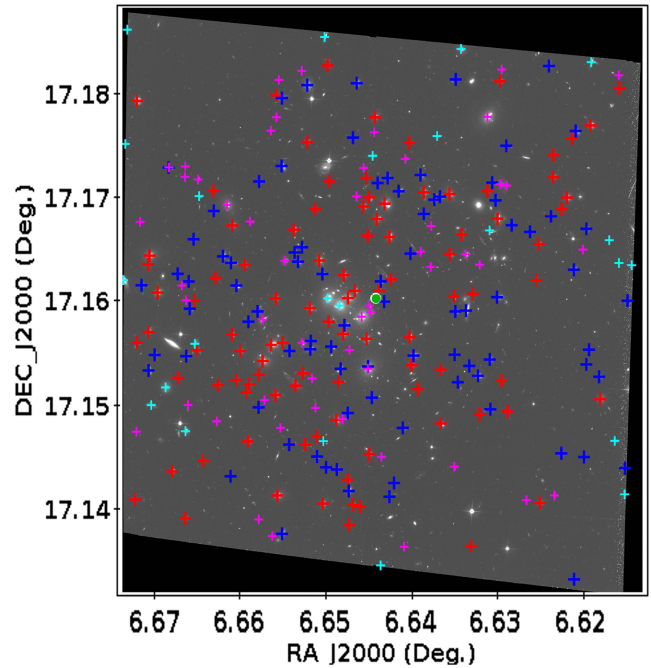


**Figure 1.** The ACS/WFC image of the ZwCl0024+1652 galaxy cluster used in this work, where east is to the left and north at the top. The centre of the cluster is indicated by a large green dot. The larger red and blue crosses indicate galaxies classified as ET and LT, respectively. While the smaller cyan crosses show those galaxies for which the probabilities are not measured and the magenta crosses show galaxies with measured probabilities but undecided morphologies (see Section 3).

16 with the ACS Wide Field Camera (WFC) using the F775W filter. The ACS/WFC has a pixel scale of  $0.05 \text{ arcsec pixel}^{-1}$  and field of view of  $202 \times 202 \text{ arcsec}^2$ . The cluster is centred at RA =  $6.64433 \text{ deg}$  and Dec. =  $17.16211 \text{ deg}$ , and the used image covers the central part of the cluster of  $\sim 1 \text{ Mpc}$ . The image data are shown in Fig. 1 with all the sources labelled.

### 2.2 WFP2 supercatalogue data

To extract redshift information and to identify cluster members, we used the public ZwCl0024+1652 master catalogue<sup>2</sup> described in Treu et al. (2003) and Moran et al. (2005). The catalogue consists of 73 318 sources, with photometric and/or spectroscopically confirmed redshifts available, and covering the area of  $0.5 \times 0.5 \text{ deg}^2$  up to the clustercentric distance of about 5 Mpc. All observations were carried out with the Canada–France–Hawaii Telescope (CFHT) and its CFH12K wide field camera, and/or the *HST* Wide Field and Planetary Camera (WFP2), as described in Treu et al. (2003). Besides redshifts, this catalogue includes the visual morphological classification of sources brighter than  $I = 22.5$  (Moran et al. 2005). We cross-matched this catalogue with our SExtractor catalogue (3515 sources) using a maximum radius of 2 arcsec. This radius was selected after testing different ones from 1 to 5 arcsec and finding it to be the best compromise between being the counterparts and having multiple matches. We obtained a total of 255 counterparts (hereafter cluster sample) with available

<sup>1</sup>Based on observations made with the NASA/ESA *HST*, and obtained from the Hubble Legacy Archive, which is a collaboration between the Space Telescope Science Institute (STScI/NASA), the Space Telescope European

Coordinating Facility (ST-ECF/ESA), and the Canadian Astronomy Data Centre (CAD/C/NRC/CSA)

<sup>2</sup><http://www.astro.caltech.edu/~smm/clusters/>

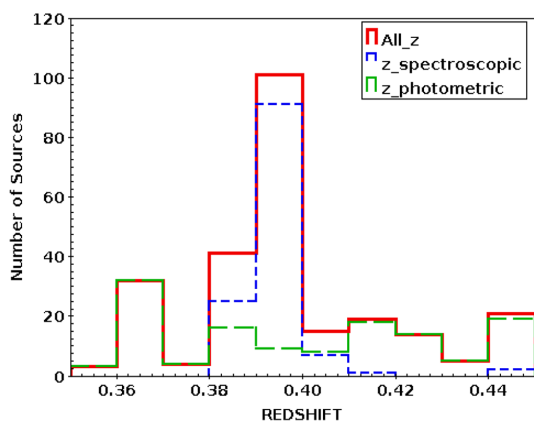


**Figure 2.** Redshift distribution of our real ZwCl0024+1652 sample where the red solid lines stand for the total sample, the blue dashed lines for spectroscopic redshifts, and the green dashed lines for photometric redshifts.

redshifts. In total, 126 and 129 sources have spectroscopic and photometric redshift measurements. The redshift distribution of the members is given in Fig. 2, including spectroscopic and photometric measurements.

### 3 MORPHOLOGICAL CLASSIFICATION

In this section we describe the morphological classification of the ZwCl0024+1652 cluster galaxies in detail. We first go briefly through the methodology used, obtained results, and final classification.

#### 3.1 Methodology

In this work we use GALSV (Huertas-Company et al. 2008) to classify galaxies morphologically in the ZwCl0024+1652 cluster. GALSV is a public code that uses a free library LIBSVM (Chang & Lin 2011) and works in an interactive data language (IDL) environment. It has been successfully tested previously, at different redshifts, and on both field and cluster galaxies (e.g. Huertas-Company et al. 2009, 2010, 2011; Pović et al. 2012, 2013, 2015; Pintos-Castro et al. 2016).

For source detection, flux extraction, and measurement of the morphological parameters we need for the morphological classification (e.g. ellipticity), we run SEXTRACTOR (Bertin & Arnouts 1996). We extracted 3515 possible sources, including cluster members and field galaxies. GALSV uses a local sample with known visual morphologies (see Section 3.2) and uses it to learn how these may be seen at redshifts and magnitude distributions of our real sample. It consists of several steps. First, it simulates local galaxies, by placing them to the redshift and magnitude distributions characteristic of the real sample. Secondly, it drops simulated local galaxies into the background that corresponds to the real sample image. Thirdly, it measures different morphological parameters (see Section 3.3), first of the simulated local sample and then of the real sample of galaxies that we want to classify. Finally, it compares morphological parameters of the training simulated local galaxies with their known visual classification and determines conditions inside the multiple-parameter space that are then applied to the real sample to be classified. The final classification is based on a number of Monte Carlo (MC) simulations, where each simulation gives a probability that the galaxy is ET. The average probability ( $P_{avg}$ ) and measured error give the final classification that the galaxy is ET.

The probability that galaxy is LT will then be  $1 - P_{avg}$ . For more details regarding GALSV see Huertas-Company et al. (2008). For applying GALSV, to include morphology determination for more fainter galaxies we took a magnitude limit of  $F775W \leq 26$ .

#### 3.2 Training sample of local galaxies

We used a catalogue of 3000 visually classified local galaxies, with known redshifts and magnitudes. The sample was selected randomly from the Nair & Abraham (2010) catalogue of visual morphology consisting of about 14 000 galaxies taken from the Sloan Digital Sky Survey (SDSS)<sup>3</sup> DR4 data. The redshift distribution of our local sample is in a range of 0.01–0.1, and most of the galaxies are bright with  $r$ -band magnitude between 13 and 17. The magnitude and redshift distributions of the training sample versus those of the real data are shown in the two plots of Fig. 3. A detailed description of the training sample can be found in Pović et al. (2013). The training sample of 3000 local galaxies was selected as a good compromise between the computing time and accuracy in classification (both being highly sensitive to the training sample size). In addition, an equal number of ET and LT galaxies were taken into account to obtain a more precise morphology, and the selected sample can be considered as representative of the whole data with respect to general galaxy properties, as shown in Pović et al. (2013).

#### 3.3 Measured morphological parameters

We used the following six parameters simultaneously to run GALSV: ellipticity (ELLIP; obtained by SEXTRACTOR), asymmetry, Abraham concentration index, GINI coefficient, M20 moment of light, and Conselice–Bershady concentration index. The last five were measured using GALSV and are briefly described as follows.

- (i) **Asymmetry (ASYM)** measures an extent to which a galaxy’s light is rotationally symmetric (Abraham et al. 1994, 1996; Conselice et al. 2003).
- (ii) **Abraham concentration index (CABR)** is defined as the ratio of fluxes of the inner isophote at 30 percent to that of the outer isophote at 90 percent (Abraham et al. 1994, 1996).
- (iii) **GINI coefficient (GINI)** is a statistical term derived from the Lorentz curve specifying the overall distribution function of the pixel values of the galaxy (Abraham et al. 2003; Lotz et al. 2004).
- (iv) **M20 moment of light** describes the second-order normalized moment of the 20 percent brightest pixels of the particular galaxy (Abraham et al. 2003; Lotz et al. 2004).
- (v) **Bershady–Conselice concentration index (CCON)** measures a light ratio within a circular inner aperture (radii comprising 20 percent of the total flux) to the outer aperture (radii containing

<sup>3</sup>SDSS is managed by the Astrophysical Research Consortium for the Participating Institutions of the SDSS Collaboration including the University of Arizona, the Brazilian Participation Group, Brookhaven National Laboratory, Carnegie Mellon University, University of Florida, the French Participation Group, the German Participation Group, Harvard University, the Instituto de Astrofísica de Canarias, the Michigan State/Notre Dame/JINA Participation Group, Johns Hopkins University, Lawrence Berkeley National Laboratory, Max Planck Institute for Astrophysics, Max Planck Institute for Extraterrestrial Physics, New Mexico State University, New York University, Ohio State University, Pennsylvania State University, University of Portsmouth, Princeton University, the Spanish Participation Group, University of Tokyo, University of Utah, Vanderbilt University, University of Virginia, University of Washington, and Yale University.

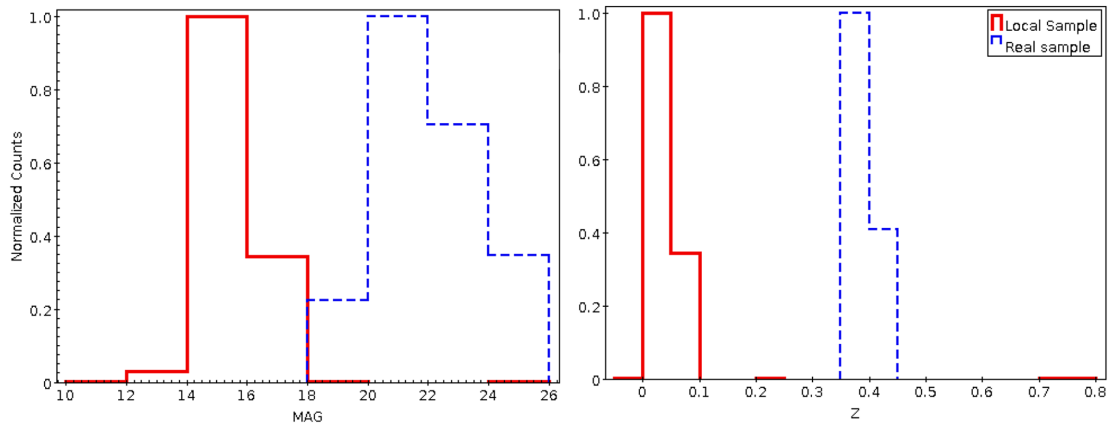


**Figure 3.** Magnitude (*right-hand plot*) and redshift (*left-hand plot*) distributions of the local training sample with known morphology (red solid lines) and the real ZwCl0024+1652 sample that should be classified (blue dashed lines).

80 per cent of the total flux) of the galaxy (Bershady et al. 2000; Conselice et al. 2000; Conselice et al. 2003).

In all measurements, the total flux is defined as the amount of flux contained within 1.5 times the Petrosian radius, where the Petrosian radius was measured with SEXTRACTOR. The centre of the galaxy is defined by minimizing the ASYM index. More details on all parameters can be found in Huertas-Company et al. (2008) and Pović et al. (2013).

### 3.4 GALSVM applied to ZwCl0024+1652

To measure the morphologies of ZwCl0024+1652 cluster members, we ran GALSVM on the *HST*/ACS F775W image described in Section 2.1 and used the SEXTRACTOR catalogue of 255 sources with all the needed input parameters and redshifts available (see Sections 2.1 and 2.2). We went through all the GALSVM steps described in Section 3.1, using the 3000 SDSS local galaxies as a training sample (see Section 3.2). We measured all the parameters described in Section 3.3 of both the training and real samples. For final classification we ran 15 MC simulations, where in each simulation we used 2000 different randomly selected local galaxies (out of 3000) with the same number of ETs and LTs. The number of MC simulations was selected as the best compromise between the computational time and accuracy of results (see Pović et al. 2013).

Taking into account previous results obtained in Pović et al. (2013), dividing a sample into different magnitude ranges can increase the accuracy of the morphological classification by optimizing the GALSVM code for fainter galaxies. Therefore, in this work we ran GALSVM three times, using the following ranges:

- (i)  $F775W \leq 22.0$  (137 galaxies),
- (ii)  $F775W \leq 24.0$  (216 galaxies), and
- (iii)  $F775W \leq 26.0$  (255 galaxies).

For each range we provided the corresponding magnitude and redshift distributions of cluster members for simulating during the classification process. These distributions are shown in Fig. 4 for both the training sample after being simulated and the real sample to be classified. For the final classification we followed the findings of Pović et al. (2013) and considered the results from the first magnitude bin, from the second bin, but only for those sources not present in the first one (for  $22.0 < \text{MAG\_AUTO} \leq 24.0$ ), and finally

from the third bin, but only for those sources not present in the previous two (for  $24.0 < \text{MAG\_AUTO} \leq 26.0$ ).

### 3.5 Final classification

In all GALSVM runs (i.e. for each magnitude bin) we obtained a final average probability from 15 MC simulations (for more details about the training sample and the running set-up see Sections 3.2 and 3.4). Finally, we obtained PROBA\_AVG<sup>4</sup> with corresponding uncertainty values for 231 galaxies out of 255. For the remaining 24 galaxies, PROBA\_AVG was not measured either because one or more parameters have values out of the respective standard range (Huertas-Company et al. 2008) or because they simply were not measured by GALSVM. Of these, 50 per cent are located on image borders, while most of the remaining sources are merging/interacting systems or some are edge-on galaxies. Only three galaxies (out of 24) have close companions, but the sample is not statistically significant for doing any additional studies. Tables 1 and 2 give the median values and  $Q1$  to  $Q3$  ranges<sup>5</sup> of the average probability  $[Q1-Q3]$ <sup>6</sup> and its error in the three magnitude bins. It can be seen that most of the brightest galaxies ( $F775W \leq 22.0$ ) are characterized by larger probability (median value  $> 0.7$ ) to be ETs, while for fainter galaxies (second and third bin) probability to be ET is lower than 0.5. As we could expect, the error values increase for fainter bins (see Table 2).

For the final classification we took into account the measured errors and considered a galaxy to be ET if  $\text{PROBA\_FINAL} = \text{PROBA\_AVG} \pm \text{PROBA\_ERR} > 0.6$  (or 0.7 in the last magnitude bin), and to be LT if  $\text{PROBA\_FINAL} < 0.4$  (or 0.35 in the last magnitude bin), where PROBA\_ERR is the uncertainty in measuring the probability and PROBA\_FINAL is the final probability after error correction. We are not able to classify galaxies with  $0.4 < \text{PROBA\_FINAL} < 0.6$  (or between 0.35 and 0.7 in the last magnitude bin) morphologically, and they will remain inside the ‘undecided class’ (UD). To define the classification boundaries, we used previous works of Pović et al. (2012, 2013) and Pintos-Castro et al. (2016). Fig. 5 shows the

<sup>4</sup>PROBA\_AVG is average probability measured by GALSVM.

<sup>5</sup> $Q1$  stands for quartile1 (25 per cent of the sample) and  $Q3$  for quartile 3 (75 per cent of the sample).

<sup>6</sup> $[Q1-Q3]$  stands for the range of values characteristic of 50 per cent of the analysed sample.

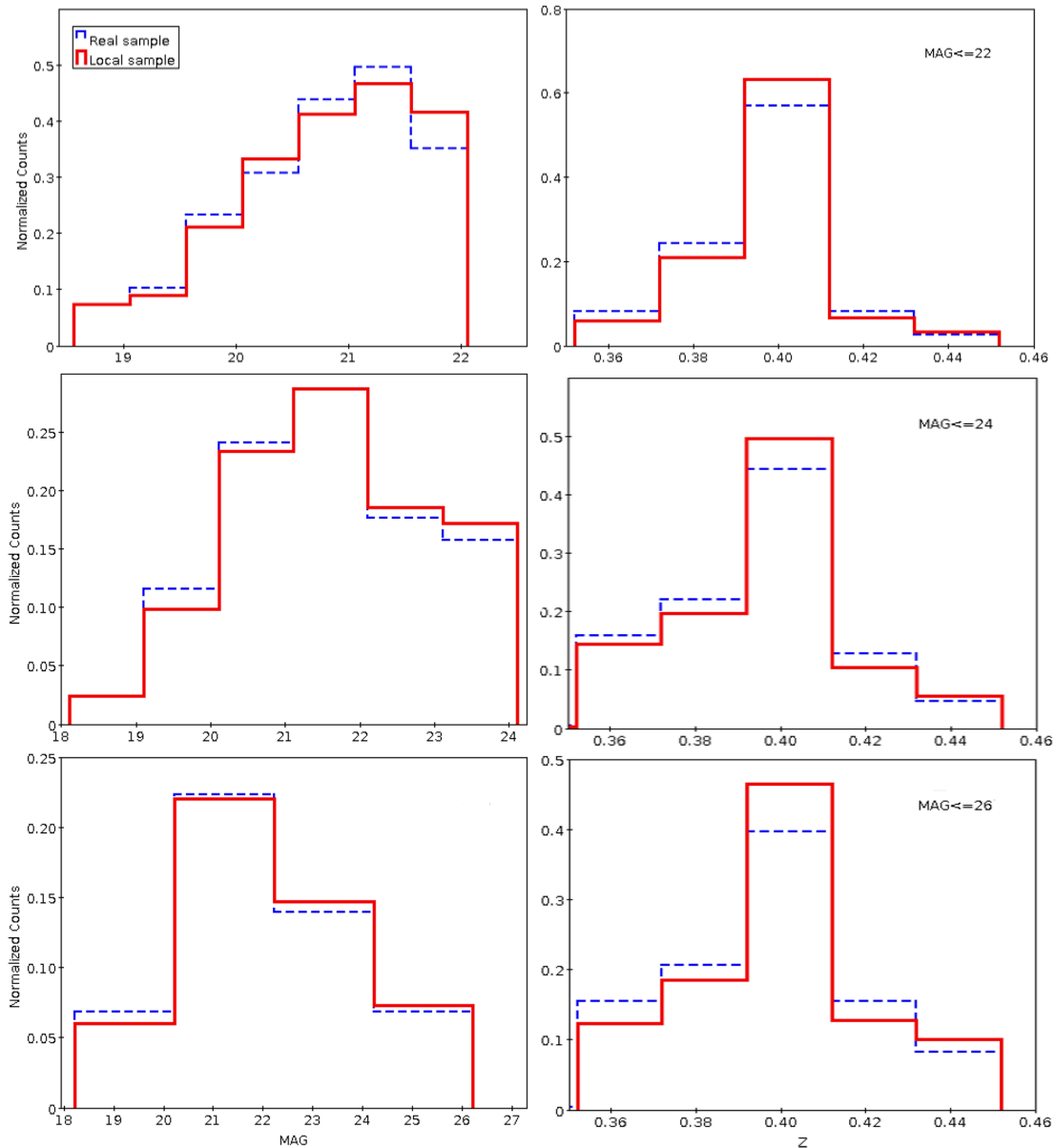


**Figure 4.** Magnitude (*left-hand plots*) and redshift (*right-hand plots*) distributions of our real data (blue dashed lines) and the simulated local sample (red solid lines). The distributions are plotted for  $F775W \leq 22.0$  (*top plots*),  $F775W \leq 24.0$  (*middle plots*), and  $F775W \leq 26.0$  (*bottom plots*).

**Table 1.** The PROBA\_FINAL values in the three magnitude ranges.

|                          | Median | [Q1–Q3]     |
|--------------------------|--------|-------------|
| $F775W \leq 22.0$        | 0.745  | 0.263–0.877 |
| $22.0 < F775W \leq 24.0$ | 0.474  | 0.170–0.727 |
| $24.0 < F775W \leq 26.0$ | 0.478  | 0.271–0.569 |

**Table 2.** The PROBA\_ERR values in the three magnitude ranges.

|                          | Median | [Q1–Q3]     |
|--------------------------|--------|-------------|
| $F775W \leq 22.0$        | 0.044  | 0.030–0.067 |
| $22.0 < F775W \leq 24.0$ | 0.045  | 0.032–0.059 |
| $24.0 < F775W \leq 26.0$ | 0.069  | 0.054–0.122 |

PROBA\_FINAL distributions in the three magnitude ranges, while the final classification is summarized in Table 3. As can be seen, out of a total of 231 galaxies with measured final probabilities, we have 97 (42 per cent), 83 (36 per cent), and 51 (22 per cent) galaxies classified as ET, LT, and UD, respectively. Fig. 6 shows the PROBA\_FINAL of the whole classified sample. We marked in Fig. 1 all the classified sources with red and blue crosses for ET and LT galaxies, respectively. Of the classified sources ET (LT) galaxies 59 (41) have spectroscopically confirmed and 38 (42) have photometric redshifts. A few bright galaxies (e.g. close to the cluster centre) remained unclassified, mainly due to the difficulty that GALSVM had with classifying galaxies in rich environments and with close companions. Moreover, it has also been deduced that only 21.6 per cent of the UD galaxies have spectroscopically confirmed redshifts while for the classified ones (ET or LT), 62.2 per cent have spectroscopic redshifts.

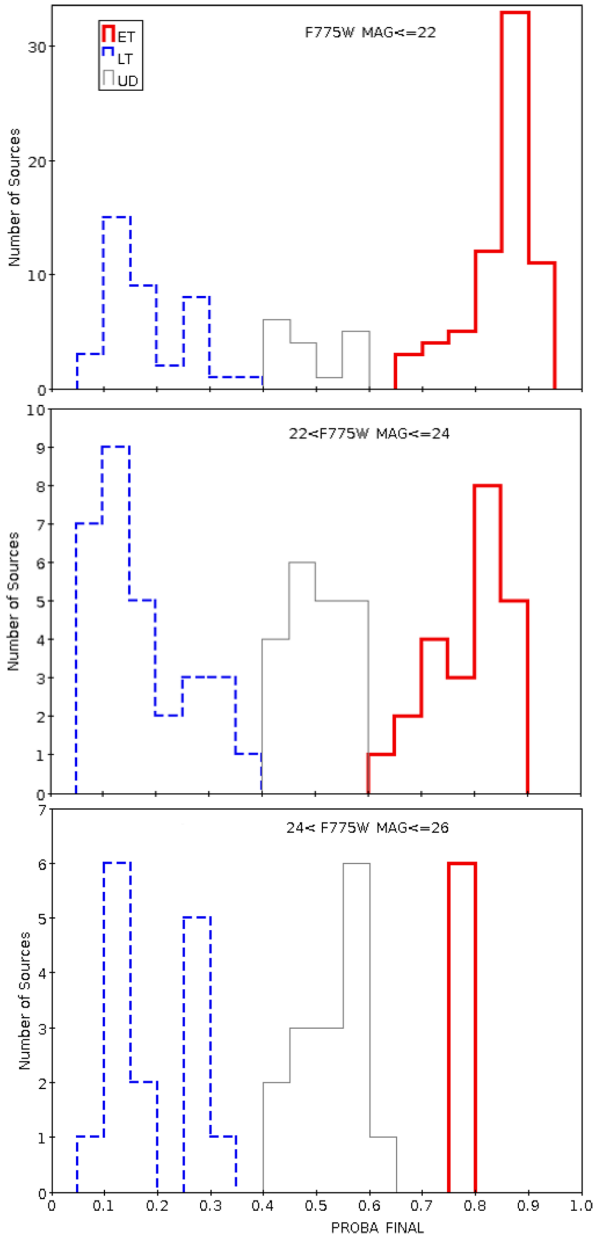


**Figure 5.** Final error-corrected probability distributions of all galaxies classified as ET (red thick solid lines), LT (dashed blue lines), and UD (grey thin solid lines) in the three magnitude ranges.

**Table 3.** Final classification of the ZwCl0024+1652 cluster members.

|                          | ET        | LT        | UD        | Total      |
|--------------------------|-----------|-----------|-----------|------------|
| F775W $\leq$ 22.0        | 68 (55%)  | 39 (32%)  | 16 (13%)  | 123        |
| 22.0 < F775W $\leq$ 24.0 | 23 (32%)  | 29 (40%)  | 20 (28%)  | 72         |
| 24.0 < F775W $\leq$ 26.0 | 6 (17%)   | 15 (42%)  | 15 (41%)  | 36         |
| <b>Total</b>             | <b>97</b> | <b>83</b> | <b>51</b> | <b>231</b> |

## 4 ANALYSIS

### 4.1 Comparisons with visual morphological classification

The visual morphological classification of 214 galaxies with spectroscopically confirmed redshifts in ZwCl0024+1652 was carried

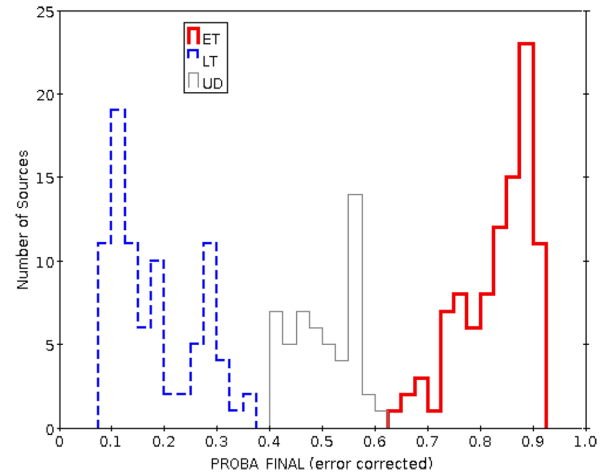


**Figure 6.** Final error-corrected probability distributions of all ET (red thick solid lines), LT (dashed blue lines), and UD (grey thin solid lines).

out previously by Moran et al. (2007), covering the clustercentric distance of 5 Mpc. In this section we compare our non-parametric classification of 231 galaxies, within the clustercentric distance of 1 Mpc (see Section 2), with the visual one. Within the region of our data ( $\sim 1$  Mpc radius) we determined that there are 123 sources with spectroscopically confirmed redshifts having visual morphology as in Moran et al. (2007), while in our sample catalogue with measured probabilities (231 sources) we have 111 sources with spectroscopic redshifts and 120 sources with photometric redshifts. We cross-matched the two catalogues using the radius of 2 arcsec and found a total 66 counterparts. The reason for a small number of counterparts is mainly the fact that the Moran et al. (2007) visual classification was done only for galaxies with confirmed spectroscopic redshifts and it only considers the best resolved galaxies. The  $I$ -band magnitude limit of galaxies in Moran et al. (2007) is 22.3, with 201 (95 per cent) of galaxies being brighter than  $I = 22$ , whereas our magnitude limit in the F775W band is 26. The  $I$ -band magnitude distribution comparison of both works is given in Fig. 7.

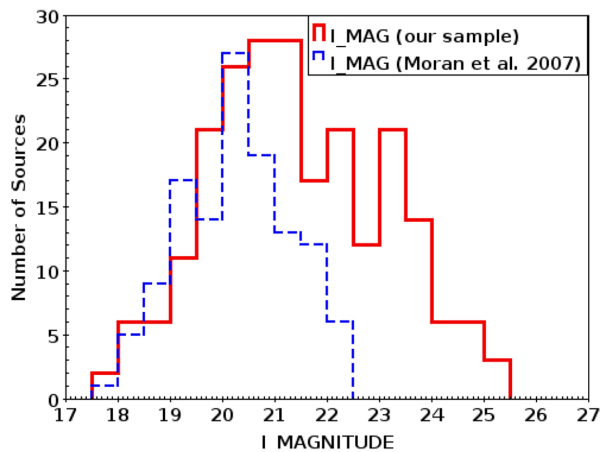


**Figure 7.** Comparison between the  $I$ -band magnitude (red solid line) of our sample galaxies classified in this work using GALSYM and the  $I$ -band magnitude of the counterparts from Moran et al. (2007) visually classified cluster members (blue dashed line).

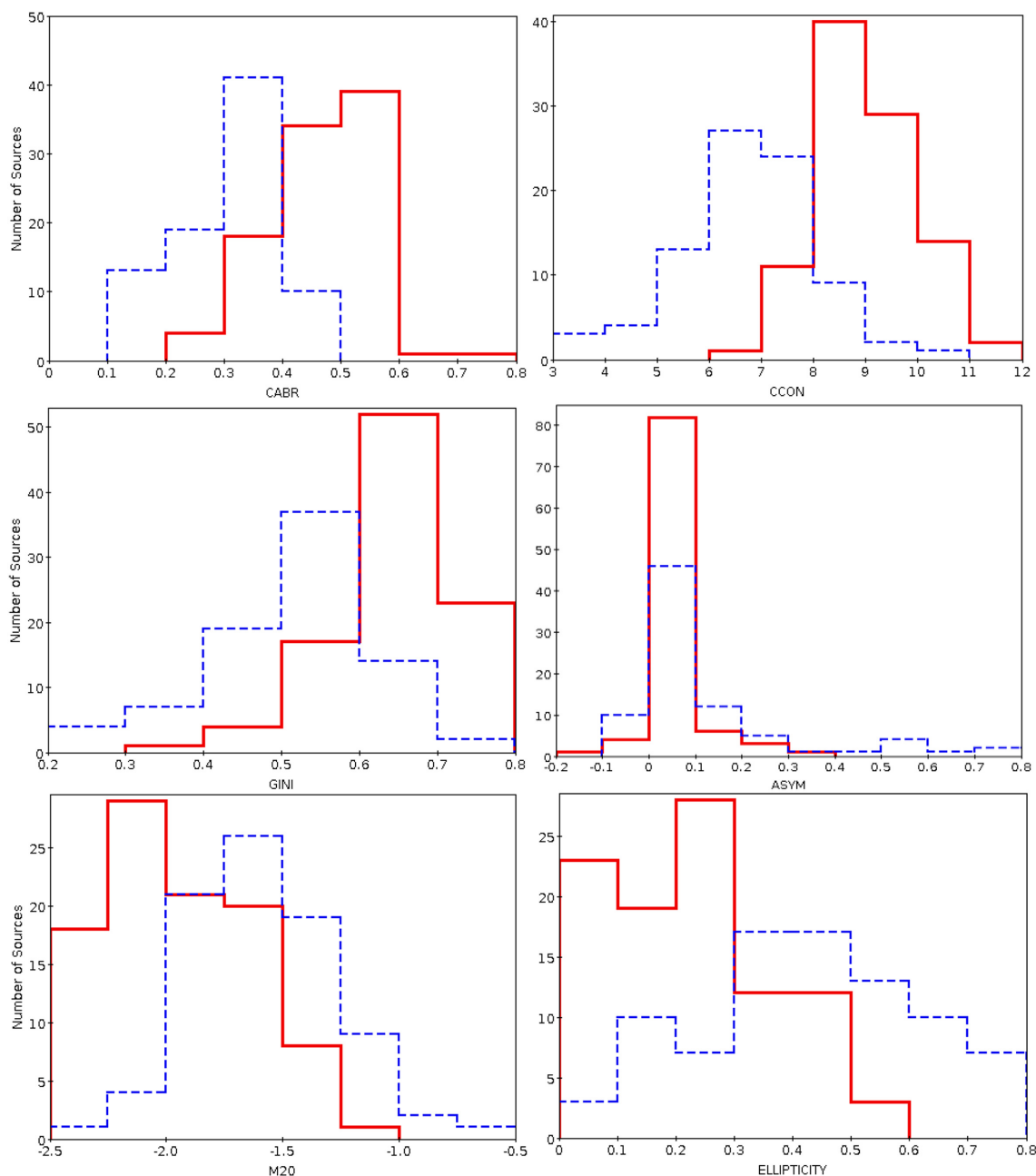


**Figure 8.** (From top left to bottom right) Distributions of CABR, CCON, GINI, ASYM, M20 moment of light, and ellipticity parameters of ET (red solid lines) and LT (blue dashed lines) galaxies.

Out of 66 counterparts, 50 and 16 galaxies were classified visually by Moran et al. (2007) as ET and LT, respectively. When compared with our results, 53 galaxies, or 81 percent, match the visual classification, of these 41 being classified as ET, and 12 as LT. Of the remaining 13 galaxies, 7 have visual classification available, but were classified as UD in our work, while for the other 6 galaxies ET/LT classification is in disagreement between the two works. Visually checking these galaxies, we found that three of them are edge-on (all being lenticulars (S0) in Moran et al. 2007, while LT in our work possibly spirals (Sa)). The other three galaxies were classified as ET in our work whereas two of them are Sa + b and one is Sc + d in Moran et al. (2007), our classification being right for one while one is observed to be an interacting system and the remaining one is a peculiar galaxy. Finally, after these

comparisons we conclude that 81 percent of our classification is in good agreement with the visual classification. Moreover, in this work we provide a reliable classification of an additional 121 galaxies within 1 Mpc of clustercentric distance, being classified for the first time.

## 4.2 Morphological parameters

The distributions of different measured morphological parameters of 180 ET and LT classified cluster members are given in Fig. 8. In addition to the histograms, Table 4 summarizes the median values of each parameter and the  $[Q1-Q3]$  range characteristic of cluster members classified as ET or LT. As can be seen from both Fig. 8

**Table 4.** Median and  $[Q1-Q3]$  range of measured morphological parameters of galaxies classified as ET or LT.

| Parameter | Measure   | ET           | LT           |
|-----------|-----------|--------------|--------------|
| CABR      | Median    | 0.493        | 0.322        |
|           | $[Q1-Q3]$ | 0.430–0.532  | 0.268–0.374  |
| CCON      | Median    | 8.894        | 6.865        |
|           | $[Q1-Q3]$ | 8.265–9.548  | 6.020–7.470  |
| GINI      | Median    | 0.650        | 0.534        |
|           | $[Q1-Q3]$ | 0.614–0.694  | 0.452–0.587  |
| ASYM      | Median    | 0.040        | 0.062        |
|           | $[Q1-Q3]$ | 0.025–0.059  | 0.021–0.158  |
| M20       | Median    | −1.996       | −1.597       |
|           | $[Q1-Q3]$ | −2.195–1.726 | −1.805–1.401 |
| ELLIP     | Median    | 0.224        | 0.433        |
|           | $[Q1-Q3]$ | 0.102–0.307  | 0.303–0.585  |

and Table 4, all the parameters follow the expected trends of ET and LT galaxies, with concentration indices such as CABR, CCON, and GINI being characterized by higher values in case of ETs, while ASYM, M20, and ELLIP are showing higher values for LTs. If we compare our results with those obtained by Pović et al. (2013), using the same methodology and data of the ALHAMBRA survey (Moles et al. 2008) in the F613W band, ZwCl0024+1652 galaxies classified as ET seem to be slightly more concentrated (in terms of all concentration indices), and characterized with lower asymmetries in the case of both ETs and LTs.

### 4.3 Morphological diagnostic diagrams

In this section, we tested some of the commonly used morphological diagnostic diagrams by comparing the measured morphological parameters. Fig. 9 shows six different diagrams and relations between CABR and ASYM, GINI, and CCON (left-hand plots, from top to bottom, respectively), and M20 and CCON, GINI, and CABR (right-hand plots, from top to bottom, respectively). These relations have been used in many previous works, showing a separation between ET and LT galaxies (e.g. Abraham et al. 1994, 1996, 2003; Conselice et al. 2000, 2003; Lotz et al. 2004; Cassata et al. 2007; Scarlata et al. 2007; Tasca et al. 2009; Pović et al. 2009, 2013; Pintos-Castro et al. 2016; Tarsitano et al. 2018).

**Table 5.** Statistical analysis of the morphological class distribution with respect to the clustercentric distance ( $R$ ), the MUMEAN, and the F775W\_MAG values. Here the median and the value range  $[Q1-Q3]$  for 50 per cent of the sources in each class to fall is computed.

| Parameter | Measure   | ET            | LT            |
|-----------|-----------|---------------|---------------|
| $R$       | Median    | 0.455         | 0.477         |
|           | $[Q1-Q3]$ | 0.308–0.623   | 0.324–0.636   |
| MUMEAN    | Median    | 22.022        | 22.120        |
|           | $[Q1-Q3]$ | 21.925–22.105 | 22.074–22.143 |
| F775W_MAG | Median    | 21.284        | 22.169        |
|           | $[Q1-Q3]$ | 20.324–22.538 | 21.384–23.492 |

It can be seen in all plots that ZwCl0024+1652 cluster members classified as ET and LT are occupying different areas on diagrams, as expected. ETs are located again in the regions characterized by higher concentrations (larger values of CABR, GINI, and CCON and lower of M20), in comparison to LTs. The ASYM parameter is much more delicate in separating sources, as has been commented previously (Pović et al. 2015), and as can be seen in Fig. 9 (top left-hand plot). However, it can be efficient in selecting interacting systems, showing larger values as can be seen in the same plot for sources with  $ASYM > 0.5$ . The relationships depicted are all in agreement with recent works (e.g. Castellón et al. 2014; Parekh et al. 2013; Pintos-Castro et al. 2016). We took into account studies of Tarsitano et al. (2018) and their fig. 11. We reproduced the Gini versus M20 diagram colour coded with CABR, CCON, ASYM, and ELLIP finding the results in line with our Fig. 9.

### 4.4 Colour–colour and colour–magnitude relations

In this section we tested the colour–colour and colour–magnitude diagrams for ZwCl0024+1652 cluster members classified as ETs and LTs. These diagrams have been tested at both lower and higher redshifts, and it is very well known that the distribution of galaxies on them is bimodal, with ETs being mainly located in the red sequence and LTs in the blue cloud (e.g. Bell et al. 2003; Cassata et al. 2007; Melbourne et al. 2007; Pović et al. 2013; Schawinski et al. 2014). In Fig. 10 we represented the relation between the  $R - K$  versus  $B - R$  rest-frame colours (left-hand plot) and between the  $B - R$  rest-frame colour and absolute magnitude in the  $B$  band (right plot). We also represent the histograms of all parameters used in the 2D plots, and their distributions for both ET and LT galaxies. In the two plots we can see the area with a higher density of ET sources, and that in general brighter and redder regions have higher fractions of ETs, as expected, while fainter and bluer parts of the diagram are populated more with LTs.

### 4.5 Morphology versus clustercentric distance

The distance between member galaxy and the centre of the cluster is calculated using the spherical law of cosines as

$$\cos(D_s) = \sin(\delta_c) \times \sin(\delta_g) + \cos(\delta_c) \times \cos(\delta_g) \times \cos(|\alpha_c - \alpha_g|), \quad (1)$$

where  $(\alpha_c, \delta_c)$  are the right ascension and declination of the cluster centre in radians, while  $(\alpha_g, \delta_g)$  are galaxy coordinates. To measure the clustercentric distance in Mpc, we used the equation :

$$R = D_{cl} \times \tan(D_s) \simeq D_{cl} \times D_s, \quad (2)$$

where  $D_{cl} = 1500$  Mpc is the distance from the observer to the cluster centre. Fig. 11 shows the distribution of clustercentric distance of 180 cluster members classified as ETs and LTs, while Table 5 provides the basic statistics (median and  $[Q1-Q3]$  ranges) of both morphological types.

We also analysed the relation between the galaxy brightness, in terms of the F775W magnitude and surface brightness (MUMEAN), and clustercentric distance, as shown in Fig. 12. For the two morphological types, Table 5 gives, again, the main statistics regarding the brightness.

Moreover, the trend of variation of the morphological fractions as a function of clustercentric distance and magnitude values have been analysed based on the plot given in Fig. 13. Finally, we analysed the

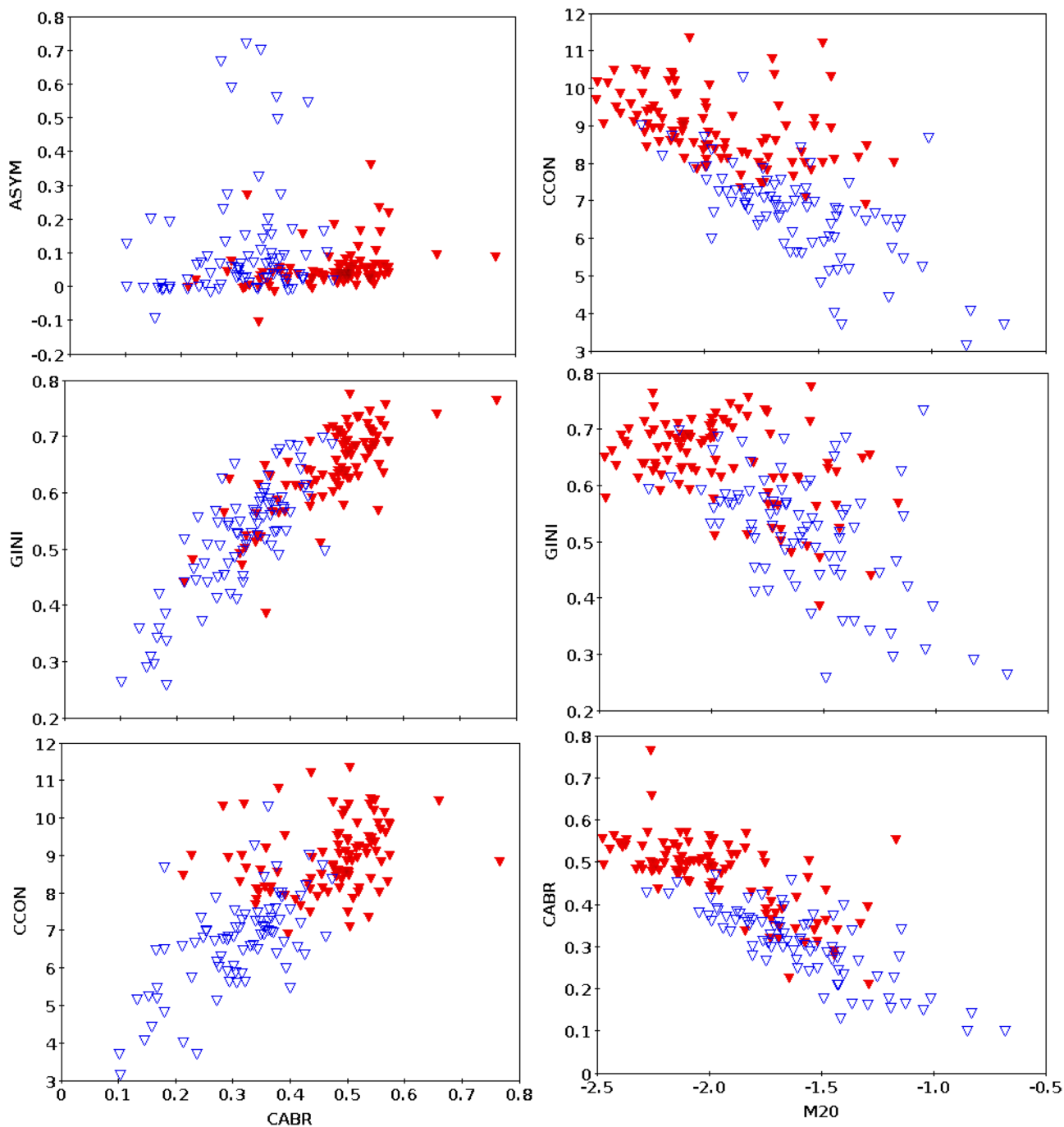


**Figure 9.** Standard morphological diagnostic diagrams showing the relation between CABR and ASYM, GINI, and CCON (left-hand plots, from top to bottom, respectively), and M20 and CCON, GINI, and CABR (right-hand plots, from top to bottom, respectively). In all the plots red solid and blue open triangles stand for ET and LT galaxies, respectively.

relation between the clustercentric distance ( $R$ ) and morphological parameters measured in the previous section. Fig. 14 shows for the first time for ZwCl0024+1652 how the six morphological parameters vary with respect to the clustercentric distance in the case of cluster members classified as ET and LT. We also selected those sources classified as LTs in this work, and which taking into account previous studies of Parekh et al. (2015) and visual inspection seem to be mergers. We discuss all plots and statistics in Section 5.

## 5 RESULTS AND DISCUSSION

### 5.1 Morphological classes

It was pointed out that the evolution of the ET proportion is affected by redshift in addition to density and clustercentric distance (Postman et al. 2005; Smith et al. 2005; Simard et al. 2009). According to the BO effect (Butcher & Oemler 1984), the LT proportion increases with redshift. This has been indifferently

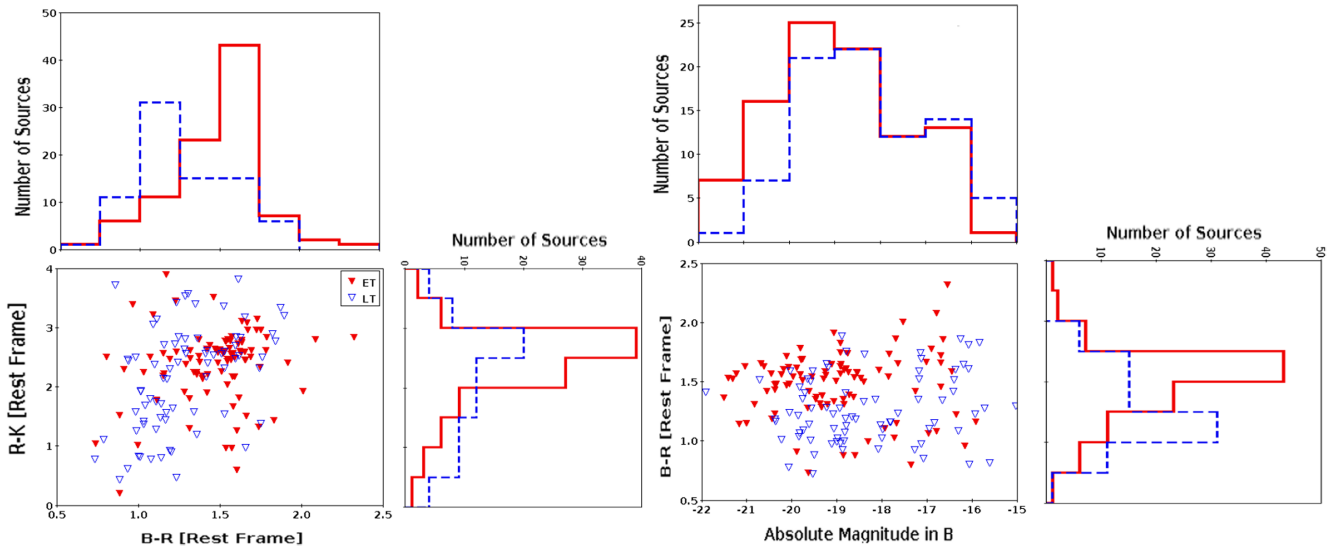


**Figure 10.** Rest frame  $R - K$  versus  $B - R$  colour–colour diagram (left-hand plot) and  $B - R$  rest-frame colour and absolute magnitude in the  $B$  diagram (right-hand plot).

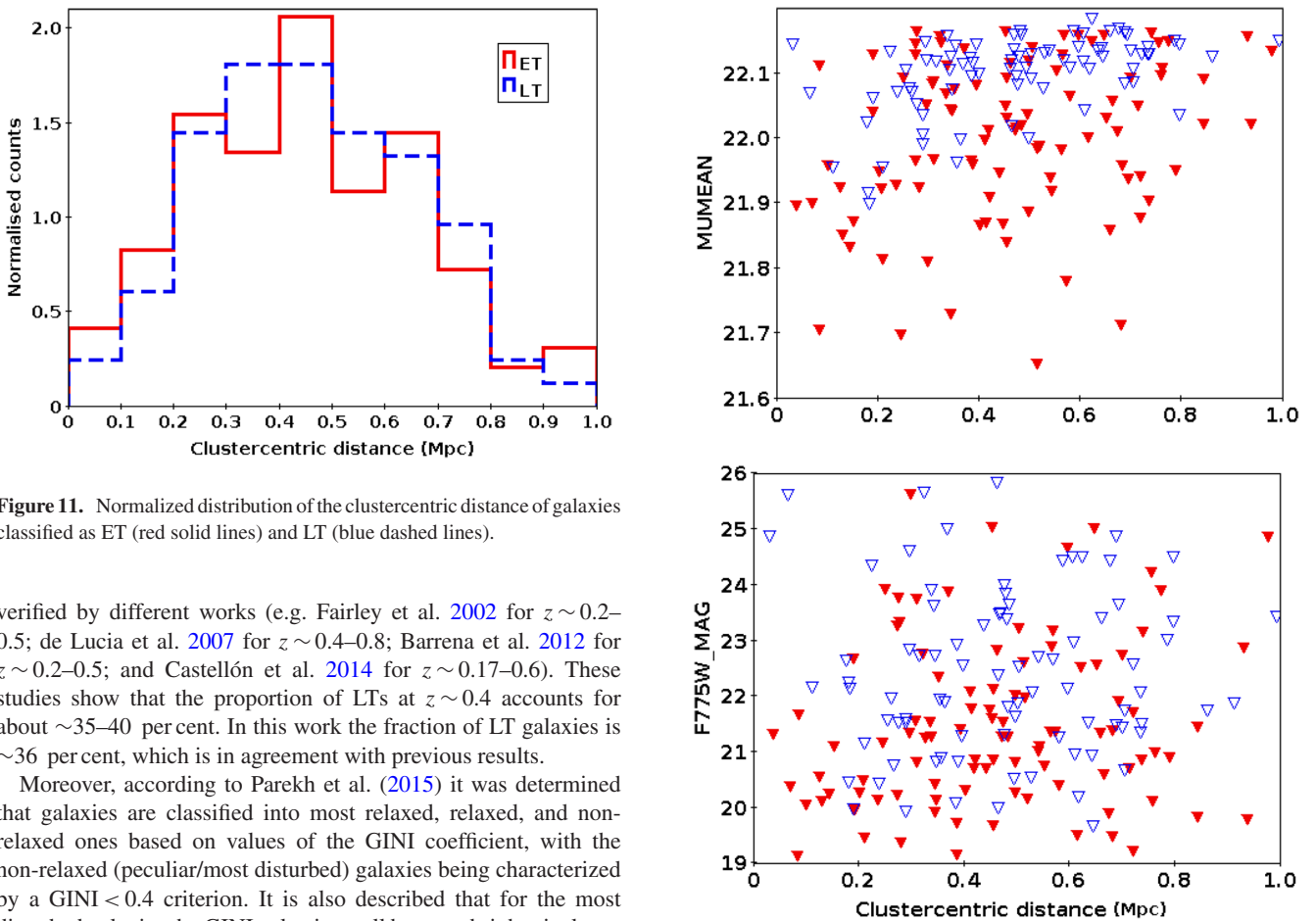


**Figure 11.** Normalized distribution of the clustercentric distance of galaxies classified as ET (red solid lines) and LT (blue dashed lines).

verified by different works (e.g. Fairley et al. 2002 for  $z \sim 0.2-0.5$ ; de Lucia et al. 2007 for  $z \sim 0.4-0.8$ ; Barrena et al. 2012 for  $z \sim 0.2-0.5$ ; and Castellón et al. 2014 for  $z \sim 0.17-0.6$ ). These studies show that the proportion of LTs at  $z \sim 0.4$  accounts for about  $\sim 35-40$  percent. In this work the fraction of LT galaxies is  $\sim 36$  percent, which is in agreement with previous results.

Moreover, according to Parekh et al. (2015) it was determined that galaxies are classified into most relaxed, relaxed, and non-relaxed ones based on values of the GINI coefficient, with the non-relaxed (peculiar/most disturbed) galaxies being characterized by a  $\text{GINI} < 0.4$  criterion. It is also described that for the most disturbed galaxies the GINI value is small because bright pixels are not compact while equally distributed in the given aperture radius. Accordingly, eight non-relaxed galaxies (peculiar) were identified from the LT class closer to the cluster core, leaving the spiral population near the core to be very small.

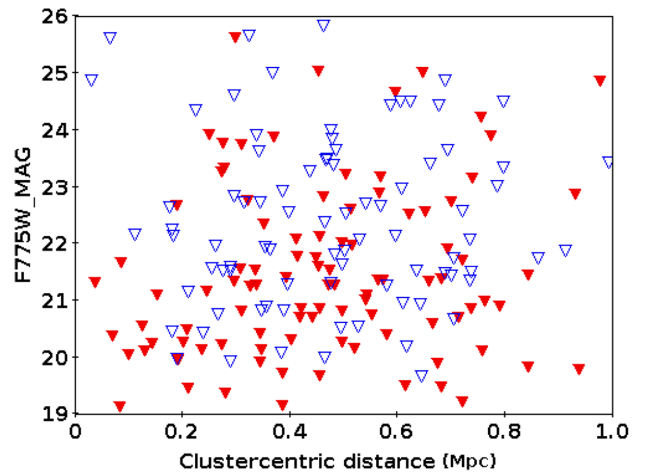


**Figure 12.** Relation between the surface brightness (top) and F775W magnitude (bottom) with clustercentric distance. For a description of the symbols, see Fig. 9.

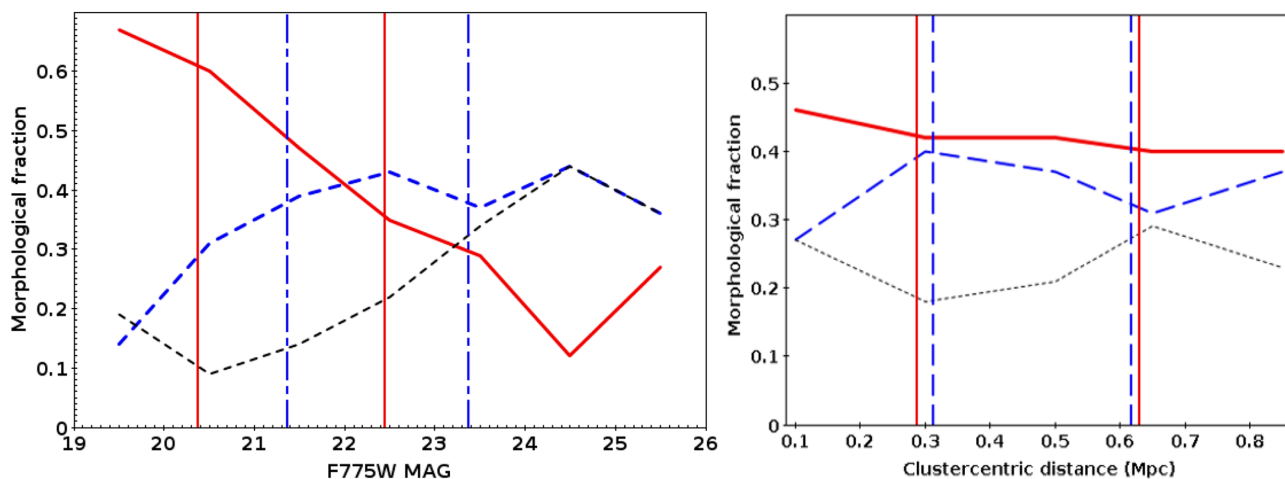


**Figure 13.** Morphological fractions as a function of F775W (*left-hand panel*) with a binning size of 1 mag and as a function of clustercentric distance (*right-hand panel*) with a binning size of 0.2 Mpc along the x-axis. The thick red plot is for the ET fraction, the blue dashed plot for the LT, and the black thinner dashed plot for the UD fraction. The thick red vertical lines indicate the  $Q1$  and  $Q3$  for the ET fraction while the dashed blue vertical lines stand for the  $Q1$  and  $Q3$  of the LT fraction.

For the overall galaxy population, Moran et al. (2007) determined that for 123 matching galaxies within the 1 Mpc region, 65.6 per cent were ET while 34.1 per cent were LT. In the same work the morphology for the MS0451–0305 galaxy cluster was determined at  $z \sim 0.5$ , with 52 per cent and 48 per cent being ET and LT, respectively. The galaxy population in our work follows nearly the same trend as what has been on board for cluster studies confirming the ET population is greater than the LT population (see Postman et al. 2005; Moran et al. 2007). As shown in Section 3.5, out of the 231 galaxies we have 42 per cent and 36 per cent galaxies classified as ET and LT, respectively.

## 5.2 Morphology versus ELGs

Using GLACE survey data, Sánchez-Portal et al. (2015) have presented a catalogue of 174 unique emission-line galaxies (ELGs) in our cluster within 4 Mpc clustercentric distance. Accordingly,  $\sim 37$  per cent of the ELGs (64 galaxies) were shown to be AGNs [broad-line AGN (BLAGN) and narrow-line AGN (NLGN)] whereas  $\sim 63$  per cent were shown to be star-forming galaxies (110 in number). Out of the 174 ELGs, 79 galaxies [52 SFs ( $\sim 66$  per cent)] and 27 AGNs ( $\sim 34$  per cent)] were within the clustercentric distance of 1 Mpc (region of concern to us). Matching the GLACE result with ours, we found 43 ( $\sim 54.4$  per cent) counterparts. Here 26 ELGs had no match in our catalogue maybe because Sánchez-Portal et al. (2015) were working only on ELGs but this is not the case for our work. Out of the matching 43 sources, 26 ( $\sim 60.5$  per cent) are SFs while the remaining 17 ( $\sim 39.5$  per cent) are AGNs. Morphologically comparing the matching ELGs, 11 galaxies ( $\sim 26$  per cent) correspond to ET, 28 galaxies ( $\sim 65$  per cent) belong to LT, and the remaining 4 galaxies ( $\sim 9$  per cent) correspond to the UD class in our results. More specifically, 18 SF galaxies are in the LT class where 5 SF galaxies fall in ET while the remaining 3 SF galaxies belong to the UD class. Similarly, for AGNs, LTs contribute 10, ETs contribute 6, while UD contributes only 1 AGN. This confirms that ELGs (SFs as well as AGNs) are mostly galaxies rather than ET galaxies.

## 5.3 Morphological fractions

In Fig. 13 we compared the morphological fraction with both the F775W magnitude and clustercentric distance. To compare it with the magnitude (left-hand plot of Fig. 13), the morphological fraction is computed for each 1 magnitude bin in such a way that a particular class fraction is the ratio of the number of a given class of galaxies to the total number of galaxies of all classes within the same bin. This, for instance, is given for the ET fraction in a given bin as

$$\text{MAG\_ET}_{\text{frac}} = \frac{\text{number of ETs}}{\text{total number of galaxies}}, \quad (3)$$

where the number of ETs  $\equiv$  ETs with magnitudes within the range of the bin and the total number of galaxies  $\equiv$  number of all galaxies (ET+LT+UD) with magnitudes in the same magnitude range.

Once it is computed for all the bins, it is plotted against the centre of the bin. It can be seen that the fraction of ET galaxies decreases as a function of increasing magnitude while that of LT galaxies increases up to F775W  $\sim 22.5$ , remaining nearly constant for fainter magnitudes. The median F775W value for ETs is determined to be 21.28 and that for LTs is 22.16, while that for UD galaxies is 23.20. Hence, we can see that the brightest galaxies are most likely to be resolved and classified into ET/LT whereas fainter galaxies could not be easily resolved, and a significant number of these galaxies are unlikely to be classified and are then left as UD. For magnitudes where F775W  $> 24.5$ , the number of sources is very small, so the statistics are too poor to draw a conclusion.

According to Fasano et al. (2012), the fraction of ET galaxies is high near the centre of a nearby cluster while decreasing as a function of clustercentric distance. The fraction of LT galaxies on the other hand is smaller closer to the core while increasing as a function of clustercentric distance (see also Zwicky 1942; Dressler 1980; Whitmore, Gilmore & Jones 1993; Pintos-Castro et al. 2016). Here, to compare with clustercentric distance (right-hand panel of Fig. 13), we compute the morphological fraction in each 0.2 Mpc bin for 0 to 0.6 Mpc, 0.1 Mpc bin for 0.6 to 0.7 Mpc, and 0.3 Mpc bin for 0.7 to 1 Mpc in the same way as in equation 3. Once it is computed for all the bins, it is plotted

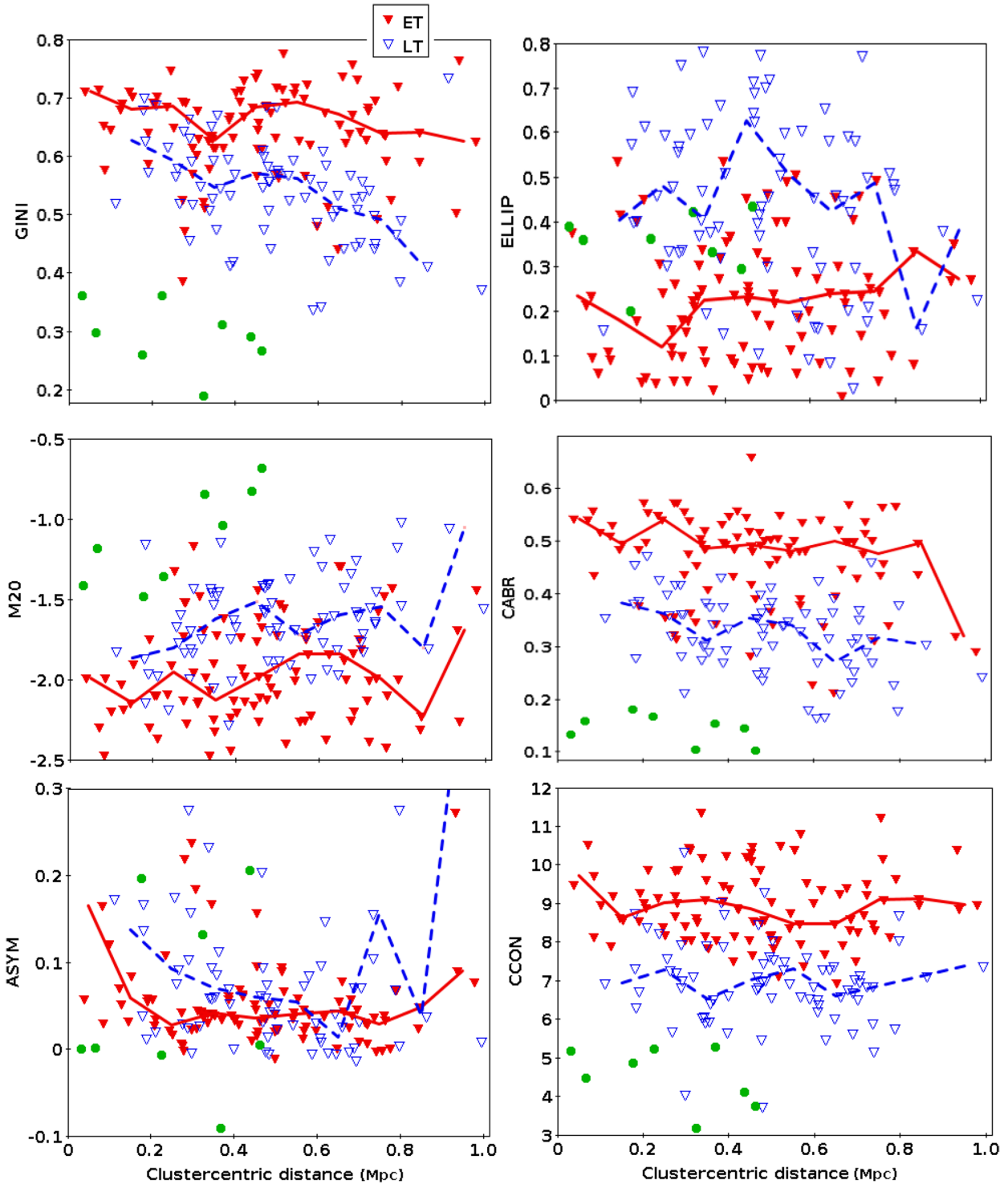


**Figure 14.** (From top to bottom, and from left to right) Relation between the GINI, ellipticity, M20 moment of light, CABR concentration index, asymmetry, and CCON concentration index and distance from the cluster centre. In all plots red solid triangles stand for ET and blue open triangles for LT galaxies. The disturbed (merging) galaxies selected from LT based on GINI < 0.4 criteria are indicated with green dots (solid circles). Median values of each parameter with clustercentric distance are shown with the red solid and blue dashed lines of ET and LT galaxies, respectively.

against the centre of the bin. Results of this work (see Fig. 11 and the right-hand plot of Fig. 13) confirm that closer to the core, the ET population fraction is higher than the LT fraction, but the ET fraction is observed decreasing and the LT fraction

increasing until the clustercentric distance of  $\sim 0.3$  Mpc, whereas beyond  $\sim 0.3$  Mpc the fractions of both populations continue nearly flat in parallel up to a clustercentric distance,  $R \sim 1$  Mpc. For clustercentric distances where  $R > 0.7$  Mpc, the number of sources

is very small, so the statistics are too poor to conclude. We can see in general that throughout the entire region the fraction of ET galaxies is consistently higher than the LT fraction and more fraction of galaxies is classified into ET/LT near the core (lower UD fraction) than at greater distances (where the UD fraction is higher) from the centre as shown in Fig. 13. Hence, our results are in a good agreement with previous results.

Moreover, out of the total number of 231 galaxies within the cluster, 111 have spectroscopically confirmed redshifts while 120 have photometric redshifts. Different trends are observed in morphological fractions throughout the clustercentric distance. It can easily be seen that for the galaxy population with spectroscopic redshifts, the ET fraction is greater than the LT fraction throughout the region, while for galaxies with photometric redshifts, the LT fraction dominates throughout over the ET fraction.

#### 5.4 Morphology–density relation

An important point to be raised is the morphology–density relation. As shown by Hoyle et al. (2012), there is a trend of an increase in the population of ET galaxies towards the cluster centre accompanied by a strong morphology–density relation. Previous studies have already described high-, intermediate-, low-density regions in a cluster (see Jee et al. 2005; Demarco et al. 2010). Analysing a cluster at  $z = 0.84$ , Nantais et al. (2013) determined that the cluster outskirts (intermediate- to low-density region) are characterized by a higher proportion of LTs (with more peculiar (merging) galaxy population than spirals), whereas a high-density region (cluster core) has a dominating ET population, few peculiar galaxies, and is almost devoid of spirals. It has been determined that near the cores of clusters the proportion of ET galaxies is  $\sim 47$  per cent, that is  $\sim 2.8$  times greater than the ET fraction in the field at the same intermediate redshift (see Delgado-Serrano et al. 2010; Nantais et al. 2013). This is a relationship that holds also for low-redshift rich clusters as determined for galaxies with redshift of  $z \sim 0.1$ – $0.2$  by Fasano et al. (2000). In our case, we were working on the broad classes (ETs and LTs), and there is no clear classification into peculiar (merging) galaxies and these will be included in our classification either in LTs or UDs. In our work, the proportion of ETs is recorded decreasing as going outwards (decreasing density) from the cluster core at least up to  $\sim 0.7$  Mpc (see the right-hand plot in Fig. 13). As mentioned previously, after  $R = 0.7$  Mpc the number of sources decreases significantly in all three morphological groups, which affects the measured fractions. Moreover, the LT population decreases approaching the cluster core, in agreement with the existing results.

#### 5.5 Relevance of morphological parameters

In Parekh et al. (2015), while working on galaxy classification into relaxed versus dynamically disturbed systems using the data of clusters at different redshifts from the *Chandra* archive, they indicated GINI, M20, and concentration as very promising parameters for identifying mergers. Accordingly, the criteria set for the most relaxed system is that  $\text{GINI} > 0.65$ ,  $\text{M20} < -2.$ , and concentration  $> 1.55$ . For the most dynamically disturbed (non-relaxed) system  $\text{GINI} < 0.4$ ,  $\text{M20} > -1.4$ , and concentration  $< 1$  were set. Intermediate between the two extreme conditions is the mildly disturbed situation. They identified that GINI is the most useful parameter in determining substructure because it does not depend on the exact position of the centre. Our classification was done with six morphological parameters (Section 3.3) to classify

the galaxies into ET and LT. Adapting the criteria from Parekh et al. (2015) for our work,  $\text{GINI} < 0.4$  gave us 12 galaxies classified into ET/LT [ET = 1 (8.3 per cent), LT = 11 (91.7 per cent)]. These 11 LT galaxies are checked visually to be the most perturbed (non relaxed) galaxies, where  $\text{M20} > -1.4$  for 9 galaxies out of the 11 LTs (with  $\sim 82$  per cent agreement). On the other hand, corresponding to  $\text{GINI} > 0.65$ , 58 galaxies were classified into ET/LT [ET = 49 (85 per cent), LT = 9 (15 per cent)] and are the most relaxed ones accordingly. Hence, our result in this aspect is subject to 85 per cent agreement with previous works (amount of ETs). But in our work,  $\text{M20} < -2.0$  is too small to be used while it is better to take the M20 cut-off for the most relaxed galaxies to be  $\lesssim -1.8$  to establish an accuracy of at least 79 per cent. Moreover, since concentration parameters are defined as in Section 3.3, from our results the cut-off values of  $\text{CABR} < 0.2$  and  $\text{CCON} < 7.0$  can be used for the most perturbed galaxies with  $\sim 91$  per cent agreement while  $\text{CABR} > 0.45$  and  $\text{CCON} > 7.5$  can segregate about  $\sim 94$  per cent of the most relaxed galaxy population. Therefore, with these cut-off limits, CCON and CABR parameters could also be equally important as GINI and M20 for the morphological classification of galaxies.

#### 5.6 Morphological parameters versus clustercentric distance

In this work, for the first time, we studied the properties of different morphological parameters in relation to the clustercentric distance ( $R$ ). In Fig. 14 we showed how GINI, ELLIP, M20, CABR, ASYM, and CCON change with  $R$  for ET and LT galaxies. In general, we do not find any clear trend in case of ASYM, CCON, and ELLIP with  $R$ . In case of GINI, CABR, and M20 a slight trend is observed of decreasing GINI and CABR showing and an increasing M20 moment of light, suggesting that as going outwards from the cluster centre the light concentration decreases. However, much better statistics are needed to confirm this result. As shown in the right-hand plot of Fig. 13 for ET class galaxies, the median and [Q1–Q3] range of  $R$  are lower on average than for LTs, and this can be explained against each parameter. This is accompanied by higher values of GINI, CCON, and CABR and lower values of ELLIP and M20, and values about zero for ASYM for ET galaxies. Whereas for LT galaxies, the median and [Q1–Q3] range of  $R$  are slightly higher on average than for ET galaxies. This can be seen from the plot describing the morphological fraction in Fig. 13. It can also be seen that the GINI value slightly decreases as a function of increasing  $R$  for LT galaxies. A similar trend is observed from the plot of CABR versus  $R$  but a very slow decrease for both classes in this case. For other parameters the values almost remain stagnant with  $R$ .

## 6 CONCLUSIONS

In this work, as part of a complete morphological study of the cluster ZwCl0024+1652 at an intermediate redshift  $z \sim 0.4$ , we presented a broad classification of member galaxies with available redshifts within the clustercentric distance of 1 Mpc using the *HST/ACS* image. We have classified galaxies up to the *I*-band magnitude of 26. By running the GALSVN code on a sample of 255 galaxies, six morphological parameters were measured and classification was provided for 231 galaxies. Of these, 111 have spectroscopic and 120 have photometric redshift measurements. From our classification and analysis we have drawn the following conclusions.

(i) Out of all the 231 galaxies 97 ( $\sim 42$  per cent) were classified as ET, 83 ( $\sim 36$  per cent) as LT, and 51 ( $\sim 22$  per cent) stayed unclassified. If we take the well-classified galaxies (180 in number), 97 ( $\sim 54$  per cent) were classified as ET whereas 83 ( $\sim 46$  per cent) fall into an LT class.

(ii) Comparing with the visual classification results in Moran et al. (2007) we have classified 53 galaxies matching with their previous visual morphologies, 6 galaxies classified to different classes, and 121 new sources that didn't have any reported morphological classification within  $\sim 1$  Mpc radius are newly classified in our work. Therefore, this work gives the most complete and largest morphological catalogue available up to now for our galaxy cluster.

(iii) Moreover, our comparison with the existing visual classification of Moran et al. (2007) is in good agreement of 81 per cent. Hence, applying GALSVN for morphological classification can be taken as a reliable technique to be used even for a large sample.

(iv) We have tested that ET and LT galaxies follow the expected distributions for different standard morphological diagrams, colour–colour and colour–magnitude diagrams.

(v) The ET morphological fraction is higher near the cluster core, decreasing outwards with the LT fraction being lower at the core and increasing outwards. Throughout the region of 1 Mpc radius, the fraction of ET galaxies is consistently greater than the LT fraction for our cluster in the region of concern to us ( $R$  out to 1 Mpc). Hence, the ET/LT fraction in the cluster is in agreement with previous studies.

(vi) Morphological fractions in our galaxy cluster at  $z \sim 0.4$  evolve with magnitude in such a way that the ET fraction dominates in the brightest magnitude limit, decreasing towards the fainter end, while the LT fraction increases as the magnitude goes fainter.

(vii) We compared our results with those of Sánchez-Portal et al. (2015) and found 43 ELG counterparts. As a result out of these counterparts, 11 galaxies ( $\sim 26$  per cent) correspond to ET while 28 galaxies ( $\sim 65$  per cent) were found to belong to LT, with the remaining 4 galaxies ( $\sim 9$  per cent) staying unclassified in our work. Moreover, with the star-forming ELGs, 18 SF galaxies are LT, 5 SF galaxies fall in ET, and the remaining 3 SF galaxies belong to the UD class. Similarly, for AGNs, LTs contribute 10, ETs contribute 6, while UD contributes only 1 AGN. Hence, in general, we deduce that ELGs are more LT in morphology than ET.

(viii) We have analysed the morphological parameters as a function of clustercentric distance out to 1 Mpc for the first time. In general we do not find any clear trend; however, better statistics would be valuable in future studies to revise the change of galaxy light concentration with  $R$ .

This work contributes significantly in the area of studies related to the evolution of galaxies in clusters involving morphological classification, and provides the most complete morphological catalogue of ZwCl0024+1652. In our future studies within the GLACE survey, we are planning to compare morphological properties with metallicities, star formation, and AGN contribution using the tunable filter data. Finally, a complete morphological catalogue that resulted from our work can be accessed with an electronic version of this paper. The first seven rows and the descriptions for all the columns are presented as an appendix in this paper.

## ACKNOWLEDGEMENTS

We acknowledge the anonymous referee for helpful comments and valuable suggestions that have significantly contributed to

improve the paper. We also thank the Ethiopian Space Science and Technology Institute (ESSTI) under the Ethiopian Ministry of Innovation and Technology (MOIT) for all the financial and technical support. ZBA specially acknowledges Joint ALMA Observatory (JAO); ESO - ALMA at Santiago, Chile for giving financial support and working space while working with M. Sanchez-Portal on the first phase of the paper. Moreover ZBA acknowledges Kotebe Metropolitan University for granting a study leave and giving material support. MP and SBT acknowledge financial support from the Ethiopian Space Science and Technology Institute (ESSTI) under the Ethiopian Ministry of Innovation and Technology (MOIT). MP also acknowledges support from the Spanish MINECO under projects AYA2013-42227-P and AYA2016-76682-C3-1-P, and from the State Agency for Research of the Spanish MCIU through the “Center of Excellence Severo Ochoa” award for the Instituto de Astrofísica de Andalucía (SEV-2017-0709). In this work, we made use of the Virtual Observatory Tool for OPERations on Catalogues And Tables (TOPCAT) and IRAF. iraf is distributed by the National Optical Astronomy Observatories, which are operated by the Association of Universities for Research in Astronomy, Inc., under cooperative agreement with the National Science Foundation. We also used ACS/HST data based on observations made with the NASA/ESA HST, and obtained from the Hubble Legacy Archive, which is a collaboration between the Space Telescope Science Institute (STScI/NASA), the Space Telescope European Coordinating Facility (ST-ECF/ESA) and the Canadian Astronomy Data centre (CADM/NRC/CSA). This work was supported by the Spanish Ministry of Economy and Competitiveness (MINECO) under the grants AYA2014-58861-C3-2-P, AYA2014-58861-C3-3-P, AYA2017-88007-C3-1-P, and AYA2017-88007-C3-2-P.

## REFERENCES

- Abazajian K. et al., 2009, *ApJS*, 182, 543  
 Abraham R. G., Valdes F., Yee H. K. C., van den Bergh S., 1994, *ApJ*, 432, 75  
 Abraham R. G., van den Bergh S., Glazebrook K., Ellis R. S., Santiago B. X., Surma P., Griffiths R. E., 1996, *ApJS*, 107, 1  
 Abraham R. G., van den Bergh S., Nair P., 2003, *ApJ*, 588, 218  
 Aniyani A. K., Thorat K., 2017, *ApJS*, 230, 20  
 Banerji M. et al., 2010, *MNRAS*, 406, 342  
 Barrena R., Girardi M., Boschin W., Mardirossian F., 2012, *A&A*, 540, A90  
 Bell E. F., McIntosh D. H., Katz N., Weinberg M. D., 2003, *ApJSS*, 149, 289  
 Bershady M. A., Jangren A., Conselice C. J., 2000, *AJ*, 119, 2645  
 Bertin E., Arnouts S., 1996, *A&AS*, 117, 393  
 Broadhurst T. et al., 2000, *ApJ*, 534, L15  
 Buitrago F. et al., 2013, *MNRAS*, 428, 1460  
 Butcher H., Oemler A., Jr, 1978, *ApJ*, 219, 18  
 Butcher H., Oemler A., Jr, 1984, *ApJ*, 285, 426  
 Cassata P. et al., 2007, *ApJS*, 172, 270  
 Chang C. C., Lin C. J., 2011, *ACM TIST*, 2, 27, Software available at <http://www.csie.ntu.edu.tw/~cjlin/libsvm/>  
 Conselice C. J., Bershady M. A., Dickinson M., Papovich C., 2000, *ApJ*, 529, 886  
 Conselice C. J., Bershady M. A., Dickinson M., Papovich C., 2003, *AJ*, 126, 1183  
 Cooper M. C. et al., 2012, *MNRAS*, 419, 3018  
 De Lucia G. et al., 2007, *MNRAS*, 374, 809  
 Delgado-Serrano R., Hammer F., Yang Y. B., Puech M., Flores H., Rodrigues M., 2010, *A&A*, 509, A78  
 Demarco R. et al., 2010, *ApJ*, 725, 1252

- Dieleman S., Willett K. W., Dambre J., 2015, *MNRAS*, 450, 1441
- Domingues S. et al., 2018, *MNRAS*, 476, 3661
- Dressler A. et al., 1997, *ApJ*, 490, 577
- Dressler A., 1980, *ApJ*, 236, 351
- Fairley B. W., Jones L. R., Wake D. A., Collins C. A., Burke D. J., Nichol R. C., Romer A. K., 2002, *MNRAS*, 330, 755
- Fasano G. et al., 2000, *ApJ*, 542, 673
- Fasano G. et al., 2012, *MNRAS*, 420, 926
- Geach J. E., Smail I., Moran S. M., Treu T., Ellis R. S., 2009, *AJ*, 691, 783
- Haines C. P. et al., 2009, *ApJ*, 704, 126
- Holden B. P. et al., 2007, *ApJ*, 670, 190
- Hoyle B. P. et al., 2012, *MNRAS*, 423, 3478
- Huertas-Company M., Rouan D., Tasca L., Soucail G., Le Fèvre O., 2008, *A&A*, 478, 971
- Huertas-Company M., Aguerri J. A. L., Tresse L., Bolzonella M., Koeke-moer A. M., Maier C., 2010, *A&A*, 515, A3
- Huertas-Company M., Aguerri J. A. L., Bernardi M., Mei S., Sanchez Almeida J., 2011, *A&A*, 525, 157
- Huertas-Company M. et al., 2007, *A&A*, 468, 937
- Huertas-Company M. et al., 2009, *A&A*, 497, 743
- Huertas-Company M. et al., 2015, *ApJS*, 221, 8
- Jee M. J., White R. L., Benitez N., Ford H. C., Blakeslee J. P., Rosati P., Demarco R., Illingworth G. D., 2005, *ApJ*, 618, 46
- Kartaltepe J. S. et al., 2012, *ApJ*, 757, 23
- Kartaltepe J. S. et al., 2015, *ApJS*, 221, 11
- Kauffmann G., White S. D. M., Heckman T. M., Ménard B., Brinchmann J., Charlot S., Tremonti C., Brinkmann J., 2004, *MNRAS*, 353, 713
- Kneib J.-P. et al., 2003, *ApJ*, 591, 53
- Kocevski D. D. et al., 2012, *ApJ*, 744, 148
- Kuminski E. et al., 2014, *PASP*, 126, 959
- Kuminski E., Shamir L., 2016, *ApJS*, 223, 20
- Lintott C. J. et al., 2008, *MNRAS*, 389, 1179
- Lintott C. J. et al., 2011, *MNRAS*, 410, 166
- Lotz J. M., Primack J., Madau P., 2004, *AJ*, 128, 163
- Lukic V., Brügggen M., Banfield J. K., Wong O. I., Rudnick L., Norris R. P., Simmons B., 2018, *MNRAS*, 476, 246
- Martini P. et al., 2013, *ApJ*, 768, 1
- Mei S. et al., 2012, *ApJ*, 754, 141
- Melbourne J., Phillips A. C., Harker J., Novak G., Koo D. C., Faber S. M., 2007, *ApJ*, 660, 81
- Moles M. et al., 2008, *AJ*, 136, 1325
- Moran S. M., Ellis R. S., Treu T., Smail I., Dressler A., Coil A. L., Smith G. P., 2005, *ApJ*, 634, 977
- Moran S. M., Ellis R. S., Treu T., Smith G. P., Rich R. M., Smail I., 2007, *ApJ*, 671, 1503
- Morrison G. et al., 1997, *AAS*, 29, 1399
- Nair P. B., Abraham R., 2010, *ApJS*, 186, 427
- Nantais J. B., Flores H., Demarco R., Lidman C., Rosati P., Jee M. J., 2013, *A&A*, 555, A5
- Natarajan P. et al., 2009, *ApJ*, 693, 970
- Nilo Castellón J. L. et al., 2014, *MNRAS*, 437, 2607
- Oke J. B., Gunn J. E., 1983, *ApJ*, 266, 713
- Parekh V. et al., 2015, *A&A*, 575, A127
- Peng C. Y., Ho L. C., Impey C. D., Rix H. W., 2002, *AJ*, 124, 266
- Peng C. Y., Ho L. C., Impey C. D., Rix H.-W., 2010, *AJ*, 139, 2097
- Pintos-Castro I., Pović M., Sánchez-Portal M., Cepa J. et al., 2016, *A&A*, 592, A108
- Pintos-Castro I. et al., 2013, *A&A*, 558, A100
- Postman M., Geller M. J., 1984, *ApJ*, 281, 95
- Postman M. et al., 2005, *ApJ*, 623, 721
- Pović M. et al., 2009, *ApJ*, 706, 810
- Pović M. et al., 2012, *A&A*, 541, A118
- Pović M. et al., 2013, *MNRAS*, 435, 3444
- Pović M. et al., 2015, *MNRAS*, 453, 1644
- Quadri R. F., Williams R. J., Franx M., Hildebrandt H., 2012, *ApJ*, 744, 88
- Reynolds J. H., 1920, *MNRAS*, 80, 746
- Sánchez-Portal M. et al., 2015, *A&A*, 578, A30
- Scarlati C. et al., 2007, *ApJS*, 172, 406
- Schawinski K. et al., 2014, *MNRAS*, 440, 889
- Sérsic J. L., 1963, *BAAA*, 6, 41
- Simard L. et al., 2009, *A&A*, 508, 1141
- Simard L. et al., 2011, *ApJSS*, 196, 11
- Simard L. et al., 2002, *ApJS*, 142, 1
- Simmons B. D. et al., 2017, *MNRAS*, 464, 4420
- Smith G. P., Treu T., Ellis R. S., Moran S. M., Dressler A., 2005, *ApJ*, 620, 78
- Tarsitano F. et al., 2018, *MNRAS*, 481, 2018
- Tasca L. A. M. et al., 2009, *A&A*, 503, 379
- The DES Collaboration, 2016, *MNRAS*, 460, 1270
- Tran K.-V. H. et al., 2010, *ApJ*, 719, L126
- Treu T., Ellis R. S., Kneib J., Dressler A., Smail I., Czoske O., Oemler A., Natarajan P., 2003, *ApJ*, 591, 53
- Wetzel A. R., Tinker J. L., Conroy C., 2012, *MNRAS*, 424, 232
- Whitmore B. C., Gilmore D. M., Jones C., 1993, *ApJ*, 407, 489
- Willett K. W. et al., 2013, *MNRAS*, 435, 2835
- Willett K. W. et al., 2017, *MNRAS*, 464, 4176
- Woo J. et al., 2013, *MNRAS*, 428, 3306
- Ziparo F. et al., 2014, *MNRAS*, 437, 458
- Zwicky I. F., 1942, *ApJ*, 95, 555

## SUPPORTING INFORMATION

Supplementary data are available at *MNRAS* online.

**Table A1.** Part of the Morphological Catalogue of galaxies in ZwCl0024+1652 Cluster.

Please note: Oxford University Press is not responsible for the content or functionality of any supporting materials supplied by the authors. Any queries (other than missing material) should be directed to the corresponding author for the article.

## APPENDIX A: THE COMPREHENSIVE MORPHOLOGICAL CATALOGUE OF GALAXIES IN CLUSTER ZWCL0024+1652 AT $z \sim 0.4$

A complete morphological catalogue of 231 sources (111 with spectroscopically confirmed redshifts and 120 with photometric redshifts) is presented in this work. This is the most comprehensive catalogue containing the morphological classes of galaxies in the ZwCl0024+1652 cluster, classified with GALSVM technique. The entire catalogue comprises a table of 231 rows standing for sources (galaxies) and 34 columns with the respective parameter for each row. In this catalogue, the morphological class is identified for 180 galaxies but the remaining 51 galaxies are marked undecided in terms of the morphological class. In addition to parameters measured in this work, SEXTRACTOR-measured photometric data and results from previous works (Treu et al. 2003; Moran et al. 2005, 2007 and Sánchez-Portal et al. 2015) are also included in this catalogue. The following are descriptions of each column of the entire catalogue.

**Column 1** ... Source index (galaxy number);

**Column 2** ... *HST* identification number of the galaxy (99.0 if not available);

**Column 3** ... Right Ascension in decimal degrees (J2000);

**Column 4** ... Declination in decimal degrees (J2000);

**Column 5** ... Ellipticity of the galaxy measured by SEXTRACTOR;

**Column 6** ... MUMEAN value for the galaxy measured by SEXTRACTOR;

**Column 7** ... Asymmetry index measured by GALSVM (described in Section 3.3);

**Table A1.** Part of the morphological catalogue of galaxies in the ZwCl0024+1652 cluster (full catalogue is available online).

| NUMBER        | <i>HST</i> .ID | RA (deg)   | DEC. (deg) | ELLIP       | MUMEAN       |
|---------------|----------------|------------|------------|-------------|--------------|
| ASYM          | CABR           | GINI       | M20        | CCON        | F775W_Mag    |
| F775W_ERR     | Redshift       | Zsource    | R (Mpc)    | PROBA_FINAL | GALAXY_CLASS |
| Visual_Morpho | ELG_Type       | B_AUTO     | V_AUTO     | R_AUTO      | I_AUTO       |
| J_AUTO        | K_AUTO         | F814W_AUTO | B_ERR      | V_ERR       | R_ERR        |
| I.ERR         | J.ERR          | K.ERR      | F814W_ERR  |             |              |
| <b>1</b>      | 80.0           | 6.62029    | 17.13273   | .2272       | 22.1522      |
| .0087         | .2443          | .3740      | − 1.5537   | 7.3720      | 23.4480      |
| .3906         | .3810          | 8          | .9763      | .3049       | LT           |
| −99.9         | −99.9          | 25.7701    | 24.9023    | 23.7896     | 23.0985      |
| 21.5017       | 19.9099        | 22.7271    | .1837      | .1923       | .0870        |
| .0974         | 99.            | 99.        | .0268      |             |              |
| <b>2</b>      | 99.0           | 6.65543    | 17.13758   | .5847       | 22.1088      |
| .5657         | .3714          | .5321      | − 1.8222   | 6.9793      | 20.7002      |
| .1101         | .3940          | 1          | .6997      | .1017       | LT           |
| −99.9         | −99.9          | 23.4553    | 22.4472    | 21.1820     | 20.3412      |
| 18.9132       | 17.3511        | 99.0       | .0251      | .0224       | .0090        |
| .0086         | .0551          | .0561      | 99.        |             |              |
| <b>3</b>      | 116.0          | 6.63273    | 17.13629   | .2521       | 22.1632      |
| −.0019        | .3118          | .4927      | − 1.5734   | 8.3250      | 23.1702      |
| .3437         | .3660          | 8          | .7356      | .7600       | ET           |
| −99.9         | −99.9          | 25.2051    | 24.4749    | 23.4430     | 22.9775      |
| 21.4379       | 19.8460        | 22.7281    | .1164      | .1378       | .0672        |
| .0924         | 99.            | 99.        | .0120      |             |              |
| <b>4</b>      | 126.0          | 6.64078    | 17.13619   | .2470       | 22.1618      |
| .0642         | .2593          | .4668      | − 1.4197   | 7.7667      | 24.5245      |
| .6413         | .3780          | 8          | .6845      | .5944       | UD           |
| −99.9         | −99.9          | 26.9703    | 26.0467    | 25.7980     | 23.5168      |
| 21.5139       | 19.9220        | 23.8584    | 99.        | 99.         | 99.          |
| .1415         | 99.            | 99.        | .0234      |             |              |
| <b>5</b>      | 9.0            | 6.66708    | 17.13923   | .3327       | 22.0930      |
| .0482         | .4381          | .5917      | − 2.2275   | 8.9588      | 21.4544      |
| .1559         | .3999          | 6          | .8261      | .7411       | ET           |
| S0            | NLAGN          | 24.1371    | 22.8917    | 21.7965     | 21.1522      |
| 20.1556       | 18.8312        | 20.9172    | .0398      | .0291       | .0136        |
| .0155         | .1482          | .1887      | .0079      |             |              |
| <b>6</b>      | 99.0           | 6.65664    | 17.13732   | .4107       | 22.1440      |
| −.0049        | .3036          | .5818      | − 1.3960   | 10.8122     | 24.0350      |
| .5118         | .4470          | 8          | .7183      | .5125       | UD           |
| −99.9         | −99.9          | 25.2620    | 25.2038    | 24.0649     | 23.5652      |
| 21.4067       | 19.8148        | 99.0       | .1260      | .2766       | .1221        |
| .1632         | 99.            | 99.        | 99.        |             |              |
| <b>7</b>      | 58.0           | 6.64736    | 17.13850   | .0849       | 22.1506      |
| −.1024        | .3391          | .5138      | − 1.8383   | 7.7022      | 22.5379      |
| .2568         | .3840          | 7          | .6226      | .6945       | ET           |
| −99.9         | −99.9          | 24.9017    | 24.1310    | 23.2602     | 22.2188      |
| 21.5017       | 19.9099        | 22.0129    | .0836      | .0950       | .0537        |
| .0435         | 99.            | 99.        | .0074      |             |              |

**Column 8** ... Abraham concentration index measured by GALSVM (described in Section 3.3);

**Column 9** ... GINI coefficient measured by GALSVM (described in Section 3.3);

**Column 10** ... M20 moment of light index measured by GALSVM (described in Section 3.3);

**Column 11** ... Bershad–Concelice concentration index measured by GALSVM (described in Section 3.3);

**Column 12** ... MAG\_AUTO (F775W) (we measured it by SEXTRACTOR for each source);

**Column 13** ... Uncertainty in MAG\_AUTO (F775W) measured by SEXTRACTOR for each source;

**Column 14** ... Redshift values for each galaxy from the public data of the ZwCl0024+1652 master catalogue generated by a team working on a ‘A Wide Field Survey of Two  $z = 0.5$  Galaxy Clusters’ (see Treu et al. 2003 and Moran et al. 2005).

**Column 15** ... Zsource [=6 from DEIMOS, 1–5: other spectroscopic sources (see Moran et al. 2007) 7 = secure photo- $z$  (see Smith et al. 2005), 8 = fairly unreliable photo- $z$  (fewer bands, fainter)];

**Column 16** ... Distance of the galaxy from the centre of the cluster (clustercentric distance) measured in Mpc;

**Column 17** ... The final probability computed taking the uncertainty (error) into account (used for morphologically classifying the galaxies in this work);

**Column 18** ... The final morphological class [Early\_Type (ET), Late\_Type (LT), or Undecided (UD)] based on the final probability value;

**Column 19** ... Visual morphology as given in Moran et al. (2007); =−99.9 if not available;

**Column 20** ... Emission line galaxy (ELG) type adapted from Sánchez-Portal et al. (2015); =−99.9 if not available;

**Columns 21–34** ... SEXTRACTOR-measured photometric data (MAG\_AUTOs and errors) for the galaxies taken from public data of the ZwCl0024+1652 master catalogue (see Treu et al. 2003;

Moran et al. 2005); =99, if not available, =−99.9 if all values not measured.

Part of the catalogue (the column values for the first seven sources) is presented in Table A1. For sample illustration, the first 7 rows of the electronic version of the catalogue with values of the columns (all the parameters) are presented here.

This paper has been typeset from a  $\text{\TeX/L\AA\TeX}$  file prepared by the author.